metals

MDPI

Review

Research and Development Progress of Laser–Arc Hybrid Welding: A Review

Yang He [1], Xinyu Song [1], Zhidong Yang [1,2,*], Ruihai Duan [1], Jiangmin Xu [1], Wenqin Wang [3], Liangyu Chen [1], Mingxiao Shi [1] and Shujin Chen [1]

[1] School of Materials Science and Engineering, Jiangsu University of Science and Technology, Zhenjiang 212003, China; a18112448895@outlook.com (Y.H.)
[2] School of Materials Science and Engineering, Harbin Institute of Technology, Harbin 150006, China
[3] School of Advanced Manufacturing, Nanchang University, Nanchang 330031, China
* Correspondence: yangzhidong@just.edu.cn

Abstract: Laser–arc hybrid welding (LAHW) is an advanced welding technology that integrates both laser and arc heat sources within a single molten pool, achieving synergistic benefits that surpass the sum of their individual contributions. This method enhances the welding speed and depth of the fusion, stabilizes the process, and minimizes welding defects. Numerous studies have investigated the principles, synergistic effects, keyhole dynamics, joint performance, and various factors influencing the parameters of laser–arc hybrid welding. This paper begins with an introduction to the classification of LAHW, followed by a discussion of the characteristics of gas-shielded welding, argon arc welding, and plasma hybrid welding. Subsequently, the welding principles underlying laser–arc hybrid welding will be elucidated. To enhance weld integrity and quality, this paper will analyze keyhole behavior, droplet transfer dynamics, welding quality performance, and the generation and prevention of welding defects that affect laser–arc hybrid welding. Additionally, a detailed analysis of the effects of residual stress on the shape, microstructure, and phase composition of the weld will be provided, along with an exploration of the influences of various welding parameters on post-weld deformation and mechanical properties.

Keywords: laser–arc hybrid welding; laser heat source; arc heat source; synergistic effect; weld defects; weld morphology

check for updates

Academic Editor: Antonio Riveiro

Received: 16 February 2025
Revised: 8 March 2025
Accepted: 14 March 2025
Published: 17 March 2025

Citation: He, Y.; Song, X.; Yang, Z.; Duan, R.; Xu, J.; Wang, W.; Chen, L.; Shi, M.; Chen, S. Research and Development Progress of Laser–Arc Hybrid Welding: A Review. *Metals* **2025**, *15*, 326. https://doi.org/10.3390/met15030326

Copyright: © 2025 by the authors. Licensee MDPI, Basel, Switzerland. This article is an open access article distributed under the terms and conditions of the Creative Commons Attribution (CC BY) license (https://creativecommons.org/licenses/by/4.0/).

1. Introduction

Laser–arc hybrid welding (LAHW) is a technique that involves the interaction between an electric arc and a laser beam within a shared molten pool. This interaction produces a synergistic effect that harnesses the advantages of both processes, thereby improving the overall quality of the weld. Previous studies have demonstrated that traditional arc-welding (AW) techniques are highly effective in bridging gaps and are particularly suitable for welding reflective materials, offering greater cost efficiency compared to those of alternative welding methods. Consequently, AW is widely adopted [1,2]. However, the welding speed in AW is constrained by the heat input and the material being welded. Exceeding the optimal welding speed can lead to uneven heat distribution, an increase in welding defects, and the distortion of the weld, requiring additional passes to ensure a uniform heat input across the joint. Moreover, the broader heat distribution in AW leads to a lower energy density compared to those of laser-welding (LW) systems, resulting in shallower weld depths and larger heat-affected zones (HAZs) [3]. As industrial sectors rapidly advance, traditional AW technologies, such as TIG (tungsten–inert gas) and MIG

(metal–inert gas)/MAG (metal–active gas), have faced challenges in meeting the growing demands for welding quality and productivity in modern engineering and manufacturing. LW is more efficient and provides deeper weld penetration compared to that of arc welding, allowing for the fusion of significantly thick materials in a single pass and achieving welding speeds unattainable by arc welding. The highly focused laser beam is predominantly employed because of its ability to reduce the heat input and minimize the weld distortion [4]. However, LW systems are costly, require precise workpiece gap and clamping accuracy, and are prone to porosity and crack defects. Additionally, the absorption rates of highly reflective materials, such as aluminum and silver, are low [5–7]. Consequently, LW is more complex to operate.

LAHW is a more efficient technique than conventional welding processes. By integrating the strengths of different heat sources, this approach effectively mitigates the limitations inherent to each individual heat source when used separately [7–9]. Figure 1 illustrates the working principle of LAHW; the laser-generated hot spot directs the arc into the keyhole, establishing a stable cathode spot that improves the arc control and significantly enhances the welding process stability. Moreover, LAHW offers several advantages, including reduced weld passes for achieving the equivalent fusion depth, a lower heat input, a smaller heat-affected zone, and reductions in porosity and crack defects. By coupling laser and arc heat sources, their complementary advantages enable the effective control of the heat input and prevention of local overheating. Furthermore, this approach mitigates the risk of localized stress concentration in the weld, caused by excessively rapid cooling. Consequently, LAHW can significantly reduce the formation of excessive residual stresses and deformation in the workpiece during the welding process [10–20]. Table 1 summarizes commonly used welding methods and their respective performances and outlines their optimal application scenarios along with the reasons for their use [20,21]. In the 1980s, Steen et al. pioneered the integration of laser welding with TIG arc welding to address challenges prevalent in laser welding at the time [22]. They found that combining laser and arc welding stabilizes the heat input, reduces angular distortion, and accelerates the welding process. The process also offers significant advantages because of its low cost and excellent stability. However, the development of hybrid welding technology has been hindered by inadequate technical conditions and high initial investment costs, limiting its industrial applications. In the 1990s, high-power lasers (e.g., CO_2 lasers) gained widespread use in hybrid welding because of their economic feasibility and favorable welding characteristics. Since then, industries such as vehicle production, shipbuilding, aerospace, and pipeline transportation have adopted this process.

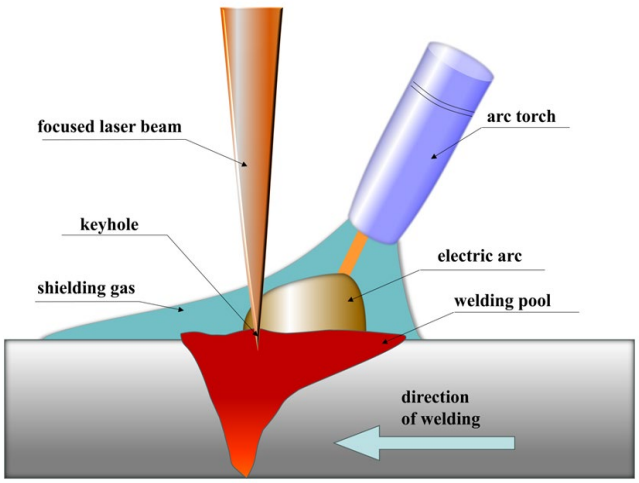


Figure 1. Schematic of the principle of LAHW, redrawn from Acherjee (2018) [21].

Table 1. Comparison of applicable materials and performances for different welding methods.

Method	Applicable Materials	Process Overview	Advantages	Disadvantages	Best Application Scenarios
LAHW	Stainless steels, aluminum, titanium, and high-strength steels	Combines laser and arc welding for deep penetration and high precision.	High speed Deep penetration Smaller HAZs	Complex control High equipment cost	Suitable for welding medium-thick and thick plates, providing excellent weld formation with minimal defects and a wide range of industrial applications.
LW	Thin metals, high-strength steels, aluminum, and non-ferrous alloys	Uses a focused laser beam for high precision with minimal heat distortion.	High precision Low distortion Fast	Limited to thin materials High initial cost	Ideal for welding thinner plates because of its high precision and low heat input, commonly used in industries such as electronics and aerospace.
PAW	Stainless steels, titanium, nickel alloys, and non-ferrous metals	Uses a focused plasma arc for high energy density and deep penetration.	High precision Deep penetration Clean welds	Complex process High operational costs	Well suited for welding difficult materials (such as titanium and nickel alloys) that require deep penetration, particularly in aerospace and high-end manufacturing sectors.
TIG	Stainless steels, aluminum, copper alloys, etc.	Non-consumable tungsten electrodes with optional filler materials.	Clean, precise welds Good for thin metals	Slow speed High skill required Porosity risk	Optimal for welding lightweight materials, thanks to its high precision, and frequently applied in aerospace, automotive, medical, and other industries.
MIG/MAG	Carbon steels, stainless steels, aluminum, etc.	Uses an electric arc and consumable electrode with shielding gas.	Versatile High deposition rate Easy automation	Larger HAZs Less precise More spatter	Ideal for thick plate welding and large-scale production, with high deposition rates, and commonly used in shipbuilding and heavy industries.

In LAHW, two heat sources are integrated in distinct ways. The first method is the arc-enhanced laser-welding process, which mitigates the limitations of the high-power laser's narrow welding range. In this method, the laser generates a keyhole in the joint, facilitating deep welding, while the arc serves as a secondary heat source, providing filler metal to enhance gap-bridging capability and expand the heat input range [23,24]. Consequently, this method is particularly suited for welding medium to thick plates, significantly reducing the occurrences of cracks and welding defects. The second method is the laser-enhanced arc-welding process, in which the arc primarily welds the metal by directing plasma vapor toward the molten pool, while the laser is used exclusively for preheating the metal and enhancing the arc-welding process. In this case, the laser's input power is substantially reduced, and the fusion depth does not experience significant enhancement. Conversely, when the laser serves as the primary heat source, the formed keyholes exhibit greater stability and minimize weld defects [25,26]. Both hybrid welding processes are significantly more complex than single processes, increasing the number of parameters that must be synchronized. Therefore, the optimal parameters for individual processes may not yield the best results for the desired hybrid weld [27,28]. Thus, accurate simulations of the

parameters are crucial in LAHW to ensure a weld with superior mechanical properties and dimensional accuracy. A common result of this interaction is that the presence of the secondary heat source reduces the laser power requirements, thereby lowering production costs [29]. However, the coupling of heat sources increases the complexity of the process, necessitating precise control and synchronization of multiple parameters. This significantly raises the demands on operators, as even minor deviations can result in defects, such as cracks or porosity. Furthermore, although the laser–arc hybrid method can initially reduce the required laser power, the necessity for complex equipment, frequent parameter adjustments, and stringent material quality standards still leads to high overall production costs. Therefore, this process still requires further improvements.

Given that LAHW involves the coupling of two distinct heat sources, the welding process is inherently more complex, presenting additional challenges. This review synthesizes literature from databases, such as Google Scholar, Web of Science, and Science Direct, utilizing search keywords, including "laser–arc hybrid welding", "LAHW", and "hybrid welding technology". The majority of the articles included are published between 2010 and 2024, encompassing the latest advancements and foundational research. Only peer-reviewed journal articles, conference papers, and patents are considered, focusing specifically on studies that discuss the development, application, or optimization of AHW technology. Irrelevant or non-peer-reviewed studies were excluded from this review. Following an initial search of approximately 500 articles, 200 were selected for detailed reading and summarization based on their quality, relevance, and contributions to the field. A comprehensive review of the literature has identified several key research areas in LAHW, including keyhole behavior, droplet transfer behavior, welding quality analysis (which encompasses residual stress analysis, microstructure analysis, and the influence of welding parameters), welding defect analysis, and industrial applications. Based on these prominent research directions, the review framework has been constructed to provide a detailed understanding of these fundamental principles and their impacts on the performance of the LAHW process. The objectives of this paper are to provide a thorough overview of the current state of LAHW applications, assess LAHW's advantages and limitations, and offer recommendations for future research. Additionally, it emphasizes the importance of LAHW in advancing industrial applications. Figure 2 outlines the specific topics covered in this review. The following section will first provide a detailed description of advanced LAHW systems, which are composed of various laser and arc sources, accompanied by an analysis of these heat sources. The third section will offer a comprehensive explanation of the principles, fundamental characteristics, and key influencing factors of heat source coupling in LAHW. In the fourth section, a thorough review of the collected literature will be presented, focusing on key phenomena in LAHW, such as keyhole behavior and droplet transition dynamics. Additionally, this section will discuss the primary factors impacting weld evaluations and weld qualities, including residual stress, microstructure, and a range of welding parameters. Finally, the fifth section will delve into the current implementation of LAHW technology across various industries, examining its practical applications and challenges. Building on the preceding introduction to laser–arc hybrid welding, this review explores the latest advancements, performance benefits, and key challenges of LAHW by examining, comparing, and summarizing research findings from various areas of recent LAHW research.



Figure 2. Framework diagram of this review [30–37].

2. Laser–Arc Hybrid Welding Technology

Laser technology can be integrated with various arc systems to develop diverse, efficient LAHW systems through parameter optimization. Table 2 summarizes the advanced combinations of laser- and arc-welding processes, outlining their respective advantages and key findings. The lasers commonly employed in welding include CO_2 lasers, Nd:YAG lasers, fiber lasers and semiconductor lasers [38–43], as shown in Figure 3A. The most widely used arc systems in LAHW are MIG/MAG and TIG. In addition to the aforementioned processes, other arc-welding techniques, such as submerged arc welding, can be combined with lasers to achieve a 1 + 1 > 2 effect. The interaction between the two heat sources produces a welding effect that surpasses that achieved by either laser or arc welding alone. However, its industrial application is limited because of the high heat input, which is more likely to cause weld deformation. CO_2 lasers consist of three primary gases: carbon dioxide (2–5%) as the active medium, nitrogen (10–55%) as the filling medium, and helium (40–88%) as the coolant [38]. Helium is the most commonly used in combination, as it reduces plasma shielding and improves laser absorption. CO_2 lasers exist as two types: continuous wave (CW) and pulsed wave (PW). Continuous-wave CO_2 lasers can deliver output powers ranging from tens of watts to tens of thousands of watts [42]. CO_2 lasers are widely employed in industrial applications because of their ability to deliver substantial output and high processing efficiency [21], with peak powers reaching millions of watts in pulsed mode [39,40]. Nd:YAG lasers are primarily produced by doping yttrium aluminum garnet (YAG) with neodymium ions. This system can operate in two modes: CW and PW [41].

Table 2. Advantages and key characteristics of different LAHW systems.

Hybrid Welding Process	Advantages	Key Findings	Ref.
Laser–MIG	The laser can be used for deep penetration welding and to enhance the welding speed, while MIG improves the arc stability, making it suitable for welding thicker materials.	Laser–MIG welded joints exhibit excellent tensile properties, with a yield strength of 326 MPa, an ultimate tensile strength of 634 MPa, and a joint efficiency of 101%, outperforming traditional welding methods.	[44]
Laser–MAG	The laser ensures deep penetration, while MAG enhances the weld strength and reduces the size of the HAZ, making it suitable for welding materials of various thicknesses.	The fusion zone (FZ) exhibits a good microstructure, which enhances mechanical properties. Additionally, the joint's tensile strength is excellent (92.5% of the base material's strength), and its toughness is also favorable.	[45]
Laser–TIG	The laser increases the welding speed and provides deep penetration welding, while TIG enhances the welding precision, making it ideal for welding thin plates and high-precision components.	Compared to traditional TIG welding, laser-induced TIG hybrid welding for aluminum alloys significantly reduces the heat input, which helps to form a finer equiaxed grain structure in the FZ relative to the base material (BM).	[46]
Laser–PAW	PAW ensures thermal penetration and allows the control of the heat input, while the laser increases the welding speed and precision. This combination enables the welding of thicker materials.	In coaxial hybrid welding, the combination of the plasma arc and laser reduces the side-cutting defects commonly seen in pure laser welding. Even at higher welding speeds, this improves weld formation and enhances gap-bridging capability.	[47]
Laser–SAW	SAW facilitates rapid deposition, with the laser providing deep penetration welding, enabling efficient welding and a smaller HAZ.	This process ensures that the tensile strengths of all the samples reach that of the base material (Rm = 762 MPa) while also preventing performance degradation because of excessive grain size.	[48]

The fundamental distinction among various lasers lies in their operating wavelengths. The Nd:YAG laser operates at a wavelength of 1.064 μm, which is comparable to that of fiber lasers. In contrast, the CO_2 laser has a wavelength of 10.64 μm, significantly longer than that of the Nd:YAG laser. Because of their shorter operating wavelengths, Nd:YAG lasers exhibit lower reflectivity on metal surfaces, enabling higher-precision laser processing at micrometer diameters [21]. Consequently, Nd:YAG lasers are more commonly used for the treatment of thin sheet metals compared to CO_2 lasers, which possess higher beam intensities and lower average powers. CO_2 lasers can achieve peak powers of up to 12,000 W, despite their low average powers [38], making them suitable for processing thick materials in industrial applications. Fiber lasers offer superior beam quality and efficiency compared to those of CO_2 lasers, increasing welding speeds by 50% to 200%, while using large amounts of Ar instead of He to reduce costs [49–51]. Like Nd:YAG lasers, fiber lasers operate at a wavelength of 1.064 μm, which enhances their effectiveness for metal absorption [37]. Additionally, the flexible structure of optical fibers facilitates

information transmission over longer distances, thereby improving laser efficiency. The optical path is encased in a protective layer, which contributes to a more stable operational environment [52]. As a result, the optimization of fiber lasers is poised to significantly influence future advancements in laser and hybrid welding technologies. Semiconductor lasers represent an advanced laser technology that offers high efficiency and compact size, delivering excellent beam quality and tunable wavelengths. Their capability to optimize power settings for various materials and processes has led to their increasing preference across diverse applications. The integration of these lasers into hybrid welding systems can enhance energy efficiency, reduce costs, and improve welding precision, particularly for thin sheet metals and high-speed production [53,54]. The following section will provide a comprehensive overview of the current LAHW technologies.

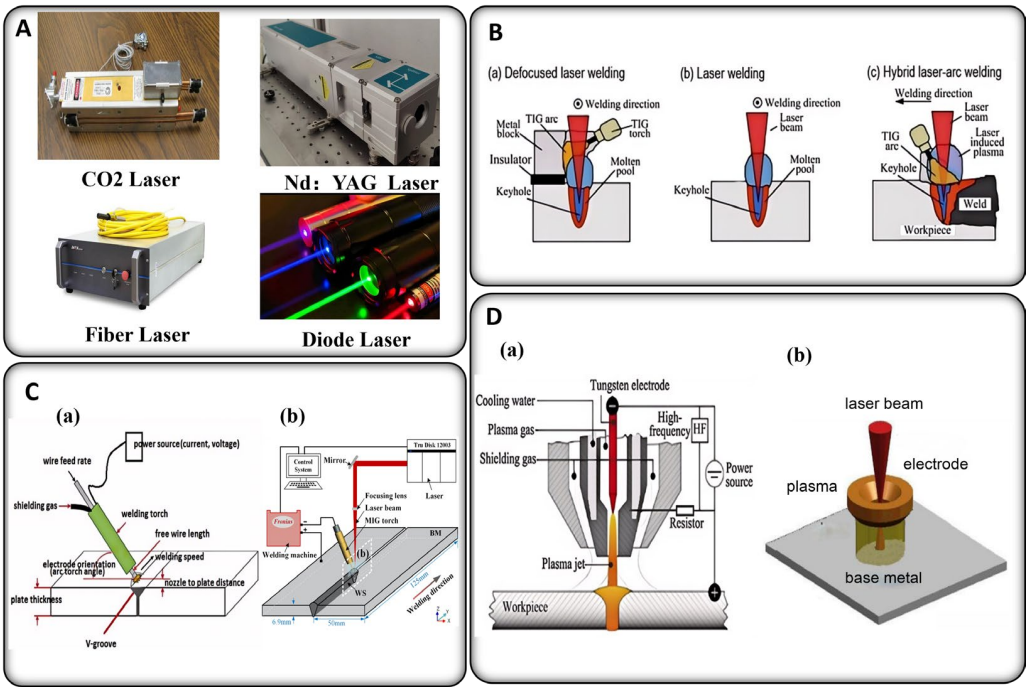


Figure 3. (**A**): Different types of lasers: carbon dioxide laser (top left), Nd:YAG laser (top right), fiber laser (bottom left), and diode laser (bottom right); (**B**) (**a**) defocused laser–TIG arc hybrid welding, (**b**) conventional LW, and (**c**) laser–TIG arc hybrid welding (HLT) [55]. Reproduced with permission from Springer Nature; (**C**) (**a**) conventional MIG [56]. Reproduced with permission from ELSEVIER, and (**b**) laser–MIG hybrid welding method (HLM) [30]. Reproduced with permission from Springer Nature; (**D**) (**a**) conventional plasma arc welding (PAW) [57]. Reproduced with permission from ELSEVIER, and (**b**) laser–plasma arc hybrid welding method [36]. Reproduced with permission from ELSEVIER.

2.1. Hybrid Laser–TIG Process

TIG employs a non-consumable tungsten electrode to achieve exceptional weld quality and versatility [58,59]. Because of its oxyphilic nature, the tungsten electrode is highly sensitive to external gases. The most commonly used shielding gases in welding are helium and argon. These inert gases serve to shield the molten pool and prevent the tungsten electrode from reacting with oxygen to form oxides [60]. Compared to other welding processes, TIG is distinguished by its ease of operation, stable welding arc, precise heat input control, and superior metallurgical quality [61]. However, TIG's single-pass welding penetration is shallow, the heat-affected zone is large, and pre-welding preparation is more complex. Additionally, the use of non-consumable tungsten electrodes requires a larger

amount of filler material during the welding process. However, excessive filler material may melt because of the high heat of the arc [62,63].

To enhance welding efficiency at a lower cost, a mode-integrating laser and TIG technologies have been employed, as shown in panel (c) of Figure 3B. The induction and compression of laser photo plasma effectively prevent arc drift and enhance the stability of the welding process [64]. This hybrid method outperforms conventional TIG welding because of the synergistic effect of the two heat sources—laser and arc—significantly increasing the melting energy during the process. Furthermore, the attraction of the laser beam to the arc plasma improves the arc stability, thereby enhancing the energy efficiency of the welding process [65,66]. Avilov investigated the variation in the current density during the hybrid laser–TIG process and found that the inclusion of the laser source results in a significantly higher arc current density compared to that of a single heat source [67]. HLT joints exhibit significantly greater strength compared to those of joints produced using either laser or TIG arc welding alone, along with finer grains and more uniform transverse residual stress [34,46]. These improvements are attributed to the laser's ability to enhance the internal structure of the weld through continuous- and pulsed-wave oscillations in hybrid welding, unlike a single heat source. However, when employing the laser–TIG technique for welding dissimilar metals, embrittlement of the welded joint may occur. To address this issue, filler metals, such as Ni, Zn, and Ti, are commonly used, and the embrittlement of welded joints can be further mitigated by applying an external energy field.

2.2. Hybrid Laser–MIG/MAG Process

This process is classified into two modes—MIG and MAG, both of which utilize gas to protect the arc and weld [68]. Its electrodes can be used continuously without replacement [69]. MIG/MAG is suitable for welding metallic materials, including high-strength steels and aluminum alloys. The low cost, continuous welding capability, and high productivity make it an excellent choice for welding applications [55,70]. However, the low fusion capacity of MIG/MAG can negatively impact welding efficiency, as it requires multiple welding passes when working with thick plates. Excessive heat input leads to a larger HAZ and greater complexity in the microstructure.

HLM can effectively manage the required amount of filler metal to enhance the gap-bridging capability, leading to higher energy utilization and efficiency. Therefore, its benefits are far superior to those of conventional MIG/MAG welding methods. Panel (C) in Figure 3 shows a comparison between conventional MIG welding and HLM, highlighting the superiority of HLM. When lasers are used in conjunction with MIG welding, shielding gases, like argon (Ar) and helium (He), are typically employed. In contrast, when paired with MAG welding, active gases, such as carbon dioxide (CO_2) and oxygen (O_2), are more commonly utilized, with shielding gases comprising mixtures of CO_2 and inert gases in various ratios [71]. Previous research has shown that employing 100% CO_2 as a reactive gas in laser–MAG hybrid welding results in welds that are virtually free from pore defects. However, the strength of these welded joints is slightly lower than that of joints welded using an Ar + CO_2 mixed shielding gas [72]. The arc is directed by the laser into the keyhole, increasing the depth of the fusion during the process. Additionally, the dilution of the arc with laser photoplasma significantly enhances laser energy absorption by the weldment. HLM is commonly used for welding medium-thick plate components, as it improves the weld quality while simultaneously increasing the welding speed [73]. For thicker weldments, a combined laser and pulsed MIG arc system can be used to achieve a single-pass full-penetration weld with reduced heat input [74]. HLM provides a more consistent heat input than standard MIG welding, facilitating grain refinement, eliminating

small hole porosity, and significantly enhancing microhardness and tensile strength [75,76]. Welded connections produced with HLM exhibit exceptional quality and are nearly defect free because of the smaller grain size in both the HAZ and the weld zone, as well as the formation of entangled grains that contribute to their overall strength [35].

Compared to other welding processes, HLM features a higher melt pool volume, which denotes a greater area of flowing molten metal. This feature enhances its gap-bridging capabilities compared to those of other hybrid welding methods [21,77]. Additionally, the weld properties can be improved utilizing various wire compositions, offering a high degree of process adaptability. These distinct advantages position the hybrid laser–MIG process as the most researched and widely applied technique in the field.

2.3. Hybrid Laser–PAW Process

The laser–plasma arc hybrid welding (HLPW) technique enhances welding efficiency and weld quality by combining laser and plasma arc welding, using the laser's high energy density and the plasma arc's high thermal stability, as shown in panel (b) of Figure 3D. PAW is a method that employs a non-self-consuming tungsten electrode. An arc with a high current density is formed by creating an arc discharge between the electrode and the base material using a tungsten electrode and an inert gas to protect the molten pool [78]. Unlike MIG, which needs numerous passes, PAW welding may be completed in a single pass for more efficient welding [21]. When compared to TIG welding, PAW has reduced heat loss, a greater energy density, and a superior weld depth-to-width ratio. However, PAW's arc energy efficiency (47–66%) is much lower than those of MIG/MAG (67–82%) and TIG (68–84%) [79,80]. This is because the PAW's keyhole mode often causes the plasma arc to extend, resulting in a higher arc loss and, hence, a fall in energy efficiency [81,82].

Laser–plasma arc hybrid welding has the benefit of efficiently reducing post-weld cooling rates by preheating the metal with the plasma arc, which increases laser absorption. As a result, when compared to other hybrid welding techniques, laser–PAW hybrid welding can enhance the welding speed while keeping the heat input constant. When a continuous-wave arc is utilized instead of a pulsed arc, the laser–PAW hybrid welding technology reduces the potential of thermal cracking in the fusion zone and allows for far wider fusion zones than laser welding. Additionally, the combined action of the laser and plasma arc helps to stabilize the arc while enhancing the weld quality. This is because the majority of the arc plasma is focused on the gap of the dielectric layer generated by the laser beam, which increases the arc's stability. Compared to laser welding, this type of hybrid welding process leads to higher mechanical strength of the welded joint. A study [83] concluded that it significantly reduces the thermal deformation caused by residual stresses, especially in the welding of aluminum alloys, which can be welded at the same time as the weldment for cathodic cleaning to remove the oxide film; the efficiency of the PAW is several times higher than that of ordinary laser welding. As a result, PAW is highly prized and commonly utilized in the welding of aluminum alloys [36]. These process and economic benefits make laser–PAW hybrid welding an attractive option for future industrial applications.

3. The Principle of the Laser–Arc Interaction

The synergetic effect of the heat sources in LAHW results from the interaction between the laser-induced plasma and the arc plasma. Figure 4A presents a schematic of this interaction. This interaction significantly influences the welding process stability, weld quality, and coupling efficiency. The presence of plasma forms a protective barrier for the laser, while its high density influences the manner in which the weldment absorbs the laser's energy. Notably, the temperature and charged-particle density of the laser-induced plasma are higher than those of the arc plasma, which results in a decrease in the charged-

particle density of the laser-induced plasma upon interaction with the arc plasma [84,85]. This reduction in density reduces laser scattering by the plasma, thereby enhancing laser absorption. Optimizing process parameters can stabilize the behavior of this interaction. Conventional laser welding typically achieves speeds exceeding 1.0 m/min, whereas arc welding generally operates at around 0.4 m/min. Increasing the welding speed beyond these ranges can result in substandard bead formation, wire melting, and process instability. The significant disparity between the two processes is further compounded by the impact of the laser-produced metal vapor on the arc's performance.

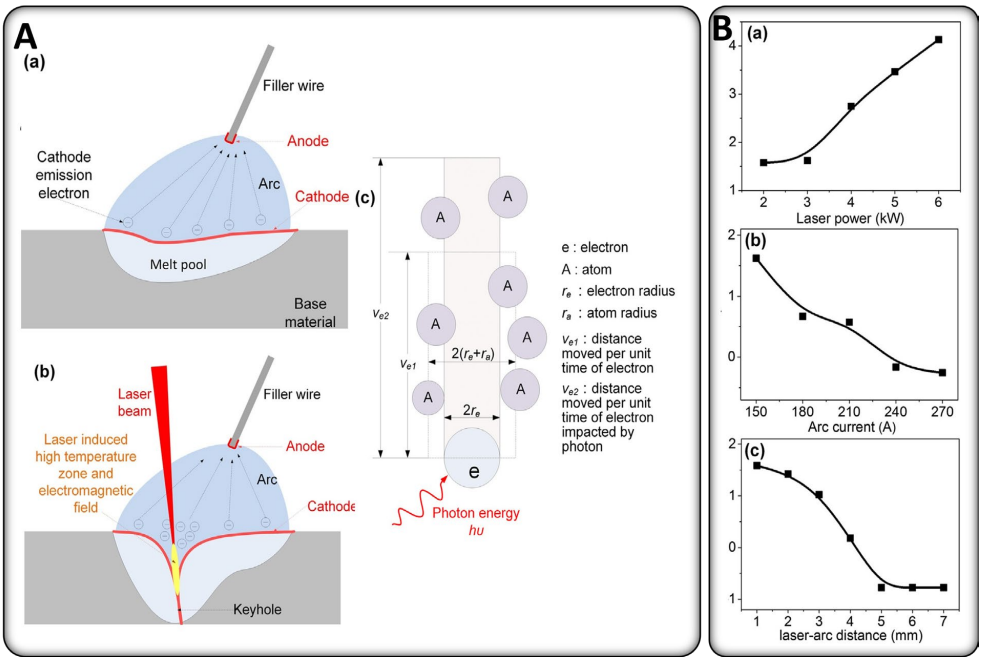


Figure 4. (**A**) Schematic representation of the synergistic effect of the heat sources [86]. Reproduced with permission from ELSEVIER: (**a**) single arc action; (**b**) role played by the laser in LAHW; (**c**) the effect of the laser on the inside of the electric arc in LAHW. (**B**) Variation in the heat sources' synergistic effect for various welding parameters [86]. Reproduced with permission from ELSEVIER: (**a**) laser power; (**b**) arc current; (**c**) D_{LA}.

The synergistic effect in hybrid welding has traditionally been assessed based on the weld surface morphology or the depth of the fusion [86]. For instance, Liu et al. examined the impact of the arc power on the depth of the fusion and assessed the level of the synergistic effect based on the magnitude of the depth of the fusion and the hardness of the weld surface [87]. However, because of the potential for errors in result evaluation, Gao et al. introduced a dimensionless parameter, known as the incremental melting energy (ψ), to represent the synergistic effect between the heat sources more intuitively. This parameter quantifies the change in the melting energy, defined as the heat required to melt both the workpiece and filler material during welding. Specifically, a greater combined influence of the heat sources results in a higher ψ value, which correlates with improved melting efficiency [88]. Building on the concept of the melting energy, Zhang et al. proposed energy utilization increments Δ_U (the energy utilization increment induced by the laser–arc synergistic effect at the same welding speed) and Δ_P (the increment of the melting depth induced by the laser–arc synergistic effect) to quantify the incremental energy utilization and depth of the fusion in the LAHW method relative to those of a single weld at the same welding speed [86]. Additionally, because the synergistic effect is strongly linked to variations in the arc current, Meng et al. quantified this effect using increments in the arc current (ψ) and found that larger variations correspond to a stronger synergistic effect.

This measurement approach offers a more intuitive demonstration of the synergistic effect of heat source coupling across various hybrid welding techniques [89]. Table 3 presents the formulae for quantifying the parameters associated with the synergistic effects, along with a critical analysis of these formulae. Figure 4A illustrates a schematic representation of this interaction. This interaction significantly influences the stability of the welding process, the quality of the weld, and the efficiency of the coupling. The presence of plasma forms a protective barrier for the laser, while its high density influences the manner in which the weldment absorbs the laser's energy. Notably, the temperature and charged-particle density of the laser-induced plasma exceed those of the arc plasma, resulting in a decrease in the charged-particle density of the laser-induced plasma upon interaction with the arc plasma [84,85]. This reduction in density reduces laser scattering by the plasma, thereby enhancing laser absorption. Additionally, the laser aids in directing the arc, while the heat produced by the arc enhances the effectiveness of the laser. This synergistic interaction results in significant improvements in welding efficiency, as demonstrated in panels (a) and (b) of Figure 4A. Optimizing process parameters can stabilize the behavior of this interaction. Conventional laser welding typically achieves speeds exceeding 1.0 m/min, whereas arc welding generally operates at around 0.4 m/min. Increasing the welding speed beyond these ranges can result in substandard bead formation, wire melting, and process instability. The significant disparity between the two processes is further compounded by the impact of the laser-produced metal vapor on the arc's performance [90].

Table 3. Parameters and formulae for quantifying the synergistic effects.

Materials and Methods	Models	Parameter Explanation	Discussion	Ref.
CO_2 Laser–MIG hybrid welding mild steel plates	$\psi = \frac{E_1-(E_2+E_3)}{E_2+E_3} \times 100\%$	E_1 is the melting energy in LAHW E_2 is the melting energy in LW E_3 is the melting energy in AW	This model simplifies the complex interaction between the laser and the arc; however, the assumption of a linear relationship for the energy variation has limited applicability, as it does not account for the influences of welding parameters and material properties on the melting energy.	[88]
Fiber laser–MIG hybrid welding AA6082-T6 Al alloy plates	$\Delta_P = \frac{P_H-(P_L+P_A)}{P_L+P_A}$	P_H is the weld penetration in LAHW P_L is the weld penetration in LW P_A is the weld penetration in AW	This formula assumes a linear relationship and ignores nonlinear effects and other factors, like the welding speed and material properties, limiting its applicability.	[86]
Fiber laser–MIG hybrid welding AA6082-T6 Al alloy plates	$\Delta_U = \frac{A_H-(A_L+A_A)}{A_L+A_A}$	A_H is the cross-sectional area of the weld in LAHW A_L is the cross-sectional area of the weld in LW A_A is the cross-sectional area of the weld in AW	This formula assumes linearity and overlooks complex interactions between the laser and arc, limiting its broader applicability under varying welding conditions.	[86]

Table 3. *Cont.*

Materials and Methods	Models	Parameter Explanation	Discussion	Ref.
Laser–MIG hybrid welding	$\dot{\psi} = \frac{I_H - I_0}{I_0} \times 100\% = \frac{\Delta I}{I_0} \times 100\%$	I_H is the statistical average current in LAHW I_0 is the statistical average current in AW	This formula assumes a linear relationship and overlooks other factors, like the plasma behavior and arc stability, which may limit its accuracy and applicability.	[89]

In LAHW, the arrangement of the laser beam and arc electrode can be classified into coaxial and paraxial configurations, primarily distinguished by the distance and alignment between the two. In a coaxial setup, the laser and arc nearly overlap along the same axis, allowing the laser to pass through the arc's center. This configuration results in highly concentrated energy and heat input, maximizing the synergistic effect of the combined heat sources. In contrast, in a paraxial arrangement, the laser and arc are positioned on separate axes or at an angle, resulting in a more independent interaction and a more flexible energy input. Although the coaxial arrangement minimizes the gap between the heat sources, enhancing the energy concentration, it may hinder the arc plasma's ability to effectively absorb the laser energy, potentially reducing the penetration efficiency and enlarging the size of the HAZ. The paraxial arrangement, on the other hand, may weaken or eliminate the synergistic effects because of the increased distance, leading to a more dispersed heat input that is more challenging to control [27]. Zou et al. found that coaxially arranged TIG arcs inhibit the formation of laser–plasma plumes, concentrate energy, and increase the depth of the fusion, thereby significantly enhancing laser energy utilization and mitigating the plume's impact on the welding process [85].

The heat source's synergy necessitates the simultaneous regulation of multiple parameters to achieve the desired effect. The key characteristics of this synergistic effect include the laser power, shielding gas parameters, and distance between the laser and the arc (D_{LA}), among others. Figure 4B illustrates the variation in the synergistic effect between the two heat sources with different welding parameters. Panel (a) indicates that the synergistic effect generally increases with higher laser powers, as the number of laser particles interacting with the arc plasma correspondingly rises. However, a complex relationship exists between the laser power and the synergistic effect. When the power exceeds a certain threshold, the increase in the laser power can lead to excessive heat input, which causes the HAZ to expand and the laser plasma to become extremely unstable. This ultimately results in a negative outcome, where the disadvantages outweigh the benefits. Panel (b) explains that as the current increases, the arc volume expands, leading to a decrease in the number of particles interacting per unit of area, ultimately weakening the synergistic effect. Panel (c) shows that as D_{LA} increases, the number of reacting particles decreases, leading to diminished concentration and a subsequent reduction in the synergistic effect. D_{LA} is essential for effective heat coupling [62]. It has been shown to influence the keyhole behavior, weld formation, and arc stability. An excessive distance can eliminate the synergistic effect, primarily affecting the behavior of the laser–arc plasma, thereby failing to meet the desired welding standards. The distribution of heat sources and the impact of D_{LA} vary depending on the material being welded. For instance, when welding materials with a high thermal conductivity, such as aluminum, it is crucial to avoid excessive heat input to prevent thermal deformation or cracking. Conversely, when welding materials with a lower thermal conductivity, such as stainless steel and titanium, the synergistic effects between the heat sources can be more advantageous, primarily through the control of the

heat input. Consequently, the distribution of the heat sources and the size of D_{LA} are mostly determined by the material properties and conditions. However, the relationship between D_{LA} and synergistic effects is complex and varies with other parameters. A high D_{LA} value may reduce the correlation between the laser and the arc, thereby weakening the synergistic effect. Conversely, it can enhance the arc's stability by reducing the plasma interference. Therefore, the optimal D_{LA} value is contingent upon the control of the welding parameters, such as the laser power and arc current. To achieve the best results, the influence of D_{LA} on the welding process should be considered alongside other factors rather than assuming a simple linear relationship, as shown in Table 3. Figure 5 shows the impact of the D_{LA} size on welding stability in the laser-guided arc mode. The blue waveform represents the welding current, while the red waveform indicates the welding voltage [91]. Panels (b–e) show that as the D_{LA} value increases from 2 to 8 mm, the arc's stability improves with increasing D_{LA} size. In contrast, panels (a) and (f) show significant fluctuations in the electrical signal, indicating a poor welding process [92]. The arc's stability was found to improve with increasing D_{LA}. However, whether D_{LA} is too large or too small, plasma disturbances increase, the arc's stability decreases, and the welding quality deteriorates. To achieve a more pronounced synergistic effect in the molten pool, the D_{LA} parameter should be regulated to the greatest extent possible [28,93]. Consequently, the effectiveness of the laser beam in reaching the molten pool and enhancing the welding efficiency relies on the precise control of the process parameters. Specifically, adjusting parameters, such as D_{LA} and the laser power, is critical, as it determines the extent to which the advantages of hybrid welding can be fully realized.

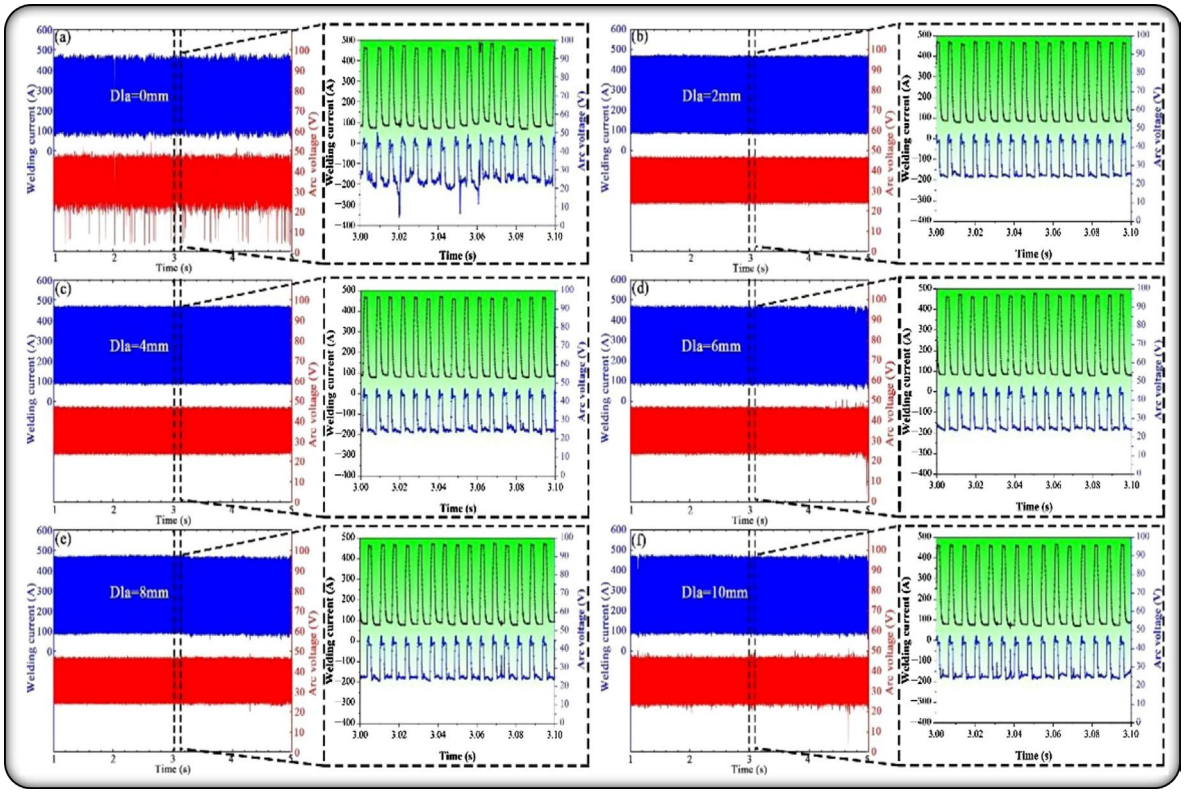


Figure 5. The voltage and current waveforms for different D_{LA} values (**a**–**f**) in laser-guided arc mode are shown, where the blue waveforms represent the welding current, and the red waveforms represent the welding voltage; when D_{LA} is either too low (**a**) or too high (**f**), the waveform exhibits instability [92]. Reproduced with permission from ELSEVIER.

4. Hybrid-Welding-Process Analysis and Quality Assessment

Parameters such as the laser power, arc energy, welding speed, welding current, welding gap, and shielding gas flow significantly influence welding phenomena and the final weld morphology in hybrid welding. This section examines the keyhole behavior and droplet transfer phenomena in LAHW to elucidate the advantages and potential improvements. By analyzing the impacts of various factors on the weld morphology and investigating the causes and prevention of welding defects, this section aims to identify associated problems and shortcomings, optimizing the hybrid welding process.

4.1. Keyhole Behavior

When a high-power, high-intensity laser is employed, the metal surface evaporates upon melting. The evaporated metal exerts recoil pressure on the surface of the molten pool, displacing the molten metal and forming a keyhole [94,95]. Figure 6A specifically illustrates the transient development of the keyhole and molten pool on the longitudinal cross-section. The keyhole behavior is critical for hybrid welding's effectiveness, as it enables energy concentration and the achievement of deep-melt welds. This process facilitates the direct delivery of laser energy to the workpiece's interior, crucial for laser-induced deep-melt welding. The keyholes formed by the laser beam retain a significant amount of the absorbed laser energy, which is then converted to heat, a phenomenon known as the keyhole effect. Consequently, deep laser-generated keyholes in hybrid welding can enhance energy utilization and improve welding efficiency [96]. When the surface tension of the keyhole and recoil pressure are nearly equal in magnitude, oscillations occur, affecting its stability [97]. This instability can lead to large bubbles forming at the keyhole's bottom. If the solidification rate of the weld metal exceeds the rise rate of the gas bubbles, weld pores form, significantly reducing the mechanical properties of the weld metal [98]. The rapid flow of the molten metal, combined with a significant metal vapor presence in the molten pool, can exacerbate keyhole instability and promote bubble formation, leading to defect development. Figure 6B illustrates keyhole collapse under unstable conditions. Panels (a) and (c) depict substantial bulges at the keyhole wall, resulting from strong molten metal flow in various materials, while panels (b) and (d) show the collapse induced by the additional flow. Following the collapse, the reduction in the keyhole depth results in a significant loss of energy absorption. Therefore, research focused on enhancing keyhole stability is essential for improving the welding efficiency.

Certain computational models can accurately predict keyhole behavior, stability, and the interaction between the laser and the molten pool in hybrid welding. Ning et al. developed a three-dimensional multiphase transient model to investigate keyhole formation and the molten pool's behavior under varying magnetic field intensities, demonstrating the model's effectiveness and accuracy through experimental and numerical comparisons [99]. However, the model's applicability is limited for materials with differing thermal conductivities, as these materials may exhibit distinct keyhole behaviors. Therefore, incorporating material-specific properties is essential to enhance the model's predictive accuracy.

Keyhole stability is significantly affected by various welding parameters [100]. A complex interplay exists between the keyhole and molten pool, where convective effects induce fluctuations in the keyholes' shapes, exacerbating keyhole instability under various welding conditions [101]. Miyagi and Ning et al. both explored the influence of varying laser strengths on keyholes. Miyagi noted that a 1 kW reduction in the laser power decreased the penetration depth, while the keyhole depth remained relatively constant, suggesting the minimal impact of the laser power on keyholes. In contrast, Ning et al. found that adjusting the laser power could effectively create piercing keyholes, facilitate excess laser energy escape, and mitigate risks from recurrent laser beam reflec-

tion, such as increased transverse shrinkage and unstable keyholes [96,102]. Excessively high laser power settings cause significant fluctuations in the recoil pressure and surface stress, adversely affecting keyhole growth and leading to instability in both keyholes and molten pools [103,104].

In addition to adjusting parameters, external methods can enhance keyhole stability. Studies have shown that magnetic-field-assisted welding effectively enhances both welding and keyhole stability [105,106]. Li et al. observed that a stable magnetic field during LW improves keyhole stability [106]. Tan et al. investigated the keyhole's dynamic behavior in the LAHW process. They discovered that in the absence of a magnetic field, the molten pool is subjected to liquid forces that press the melt against the back wall of the keyhole, resulting in the formation of a keyhole hump and increasing the likelihood of collapse. Conversely, under the influence of a magnetic field, the rear wall of the keyhole undergoes reduced distortion, thereby decreasing the likelihood of collapse, as illustrated in Figure 6C [99]. Zhan et al. used the law of the change in the keyhole depth over time under a magnetic field influence to demonstrate its effect on melting pools' stability. Their results indicated that achieving a consistent keyhole depth in a shorter duration is feasible [107]. Liu et al. investigated the keyhole's dynamic behavior in HLM with varying magnetic flux densities. They discovered that at a sufficiently high magnetic flux density, the droplet migrates away from the keyhole's melt pool because of the magnetic field force, avoiding the collision and influence [108]. Several parameters, including the welding conditions, surrounding environment, and mechanical impacts, must be considered to maintain keyhole stability and prevent defects, such as spatter and porosity, during this process.

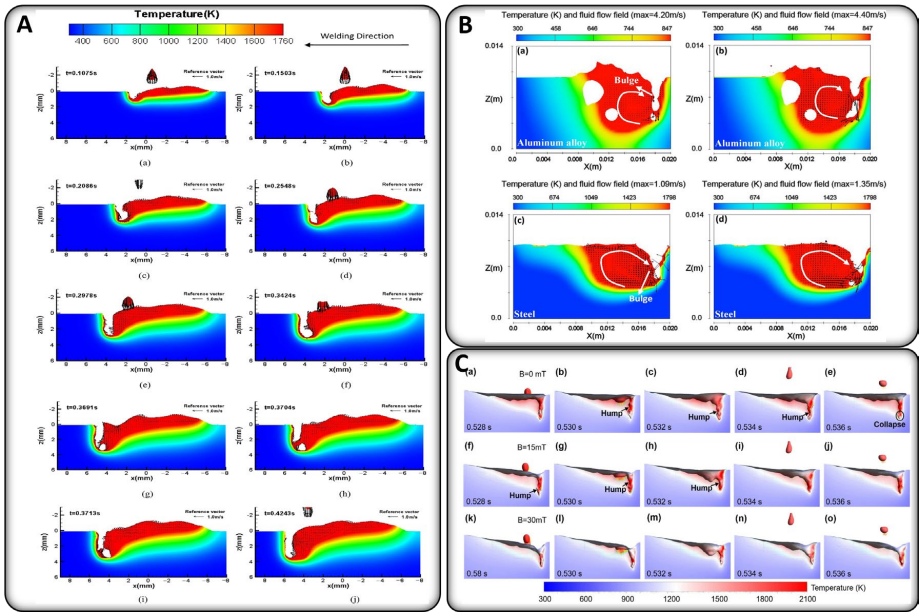


Figure 6. Dynamic evolution analysis of a keyhole in a molten pool [97]. Reproduced with permission from ELSEVIER: (**A**) Schematic diagram of the keyhole evolution in the melt pool; (**B**) schematic diagram of keyhole collapse during this process [109]. Reproduced with permission from ELSEVIER: (**a**) aluminum alloy at 0.245 s and (**c**) steel at 0.264 s show the initial stage of the keyhole collapse, with bulging formation at the keyhole's rear wall for different materials; (**b**) aluminum alloy at 0.250 s and (**d**) steel at 0.270 s indicate the later-stage collapse between the bulge and the keyhole's front wall. (**C**) Schematic diagram of the dynamic evolution of keyholes during the LAHW process [99]. Reproduced with permission from ELSEVIER: (**a**–**e**) magnetic field strength of 0 mT; (**f**–**j**) magnetic field strength of 15 mT; (**k**–**o**) magnetic field strength of 30 mT. Comparison shows that without the influence of a magnetic field, the stability of the keyhole in the LAHW process is very poor.

4.2. Droplet Transfer Behavior

Melt droplet transfer significantly impacts the welding process stability and weld quality [110]. The arc's heat melts the wire's resistive tip into metal droplets, which are then transferred to the molten pool along the wire's centerline. If the droplets fail to enter the molten pool, excessive spatter can occur, compromising the weld quality. In LAHW, the molten droplet transfer behavior provides crucial insights into arc characteristics, melting efficiency, and the welding process itself [111]. Numerous studies have shown that the melt droplet transfer behavior significantly influences the weld stability, spatter, and overall quality [32,112,113]. A combination of forces—gravity, surface tension, and electromagnetism—affects the transfer mode and stability.

Figure 7A presents the force state diagram of a molten droplet during LAHW. Gravity acts as a downward force, facilitating droplet transmission. Electromagnetic force is the primary factor influencing the droplet transfer. Surface tension prevents the molten metal from detaching from the wire's tip, acting as a retention force that impedes the droplet transfer. The forces acting on the droplet significantly influence the weld formation, microstructure, and quality, with the transfer mode closely linked to the molten pool's stability. This makes it a critical parameter in the welding droplet transfer [114,115]. Melt droplet transfer modes include short-circuit, globular, and spray transfers. The droplet transfer mode significantly influences the weld quality and stability. The three droplet transfer modes in LAHW are shown in panels (e) and (f) in Figure 7B [111,116]. When the arc current is low, unseparated droplets contact the molten pool, forming a short-circuit liquid bridge indicative of short-circuit transfer. Gao et al. evaluated the molten pool status in real-time during LAHW and found that extended short-circuit transfer duration correlates with increased process instability [117]. In globular transfer, which occurs at a long arc length and a low current, the wire tip generates droplets larger than the diameter of the wire. These droplets fall into the molten pool because of gravitational forces. In this mode, the larger size of the droplets often leads to defects, such as spatter or an enlarged HAZ. In contrast, spray transfer involves droplets that flow along the wire into the molten pool at specific arc lengths and higher welding currents. Transitioning to spray transfer reduces droplet spatter and its effect on the molten pool, significantly enhancing the welding stability. Various factors influence the droplet transfer mode. In the horizontal position, the electromagnetic force promotes droplet transfer, while gravity causes the droplet to fall; in the vertical position, the electromagnetic force inhibits droplet transfer, resulting in the short-circuit transfer mode [118].

Proper regulation of welding parameters and external conditions can ensure smooth and consistent droplet transfer during hybrid welding, reducing heat input losses and enhancing stability. Welding speed influences energy density, which is directly related to metal vapor generation. Metal vapor generates high-speed airflow within keyholes, creating a vertical reaction force that impedes droplet transfer [112]. Liu et al. observed that as the welding speed increases, both the duration and size of the droplet formation decrease, leading to a more stable transfer mode, as illustrated in Figure 8. Liu et al. conducted experiments on 8 mm thick 316L stainless steel plates using LAHW. They found that the addition of the laser promoted the droplet transfer behavior, as it improved the arc's conductivity. When the laser power increased from 0 kW to 5 kW, as shown in Figure 9, it accelerated the droplet transfer behavior and increased the welding wire's deposition rate [33]. In Jing's experiments, high-speed imaging and laser diagnostics were employed to effectively detect the droplet movement process. However, high-speed imaging may encounter challenges under high-temperature conditions, which could impact the accuracy of the measurements. Nonetheless, it remains a reliable method, and by combining both techniques, the droplet transfer behavior can be accurately detected, allowing for a thorough

analysis of its stability [119,120]. The laser's arrangement relative to the arc significantly influences whether the laser directly irradiates the arc. When coaxial, the laser is directed toward the arc, forming large droplets and considerable spatter. In contrast, in a paraxial configuration, the laser does not directly irradiate the droplet, and the arc dilutes the laser-induced plasma, increasing the laser absorption. However, as D_{LA} increases, the laser and arc separate, causing instability in the molten droplet transfer [86]. Figure 10 illustrates the effect of varying magnetic field intensities and frequencies on the droplet transfer. The figure shows that applying the magnetic field suppresses droplet spattering and instability. Additionally, as the frequency increases, the droplet transfer exhibits improved arc stability, as indicated in (c). If these parameters are not properly configured, arc droplets may impact the molten pool, causing defects, like keyhole collapse, spatter, and dents. Therefore, both welding parameters and external variables significantly influence the droplet transfer mode and stability. Consequently, multiple factors must be considered simultaneously to ensure stable and smooth droplet transfer [121].

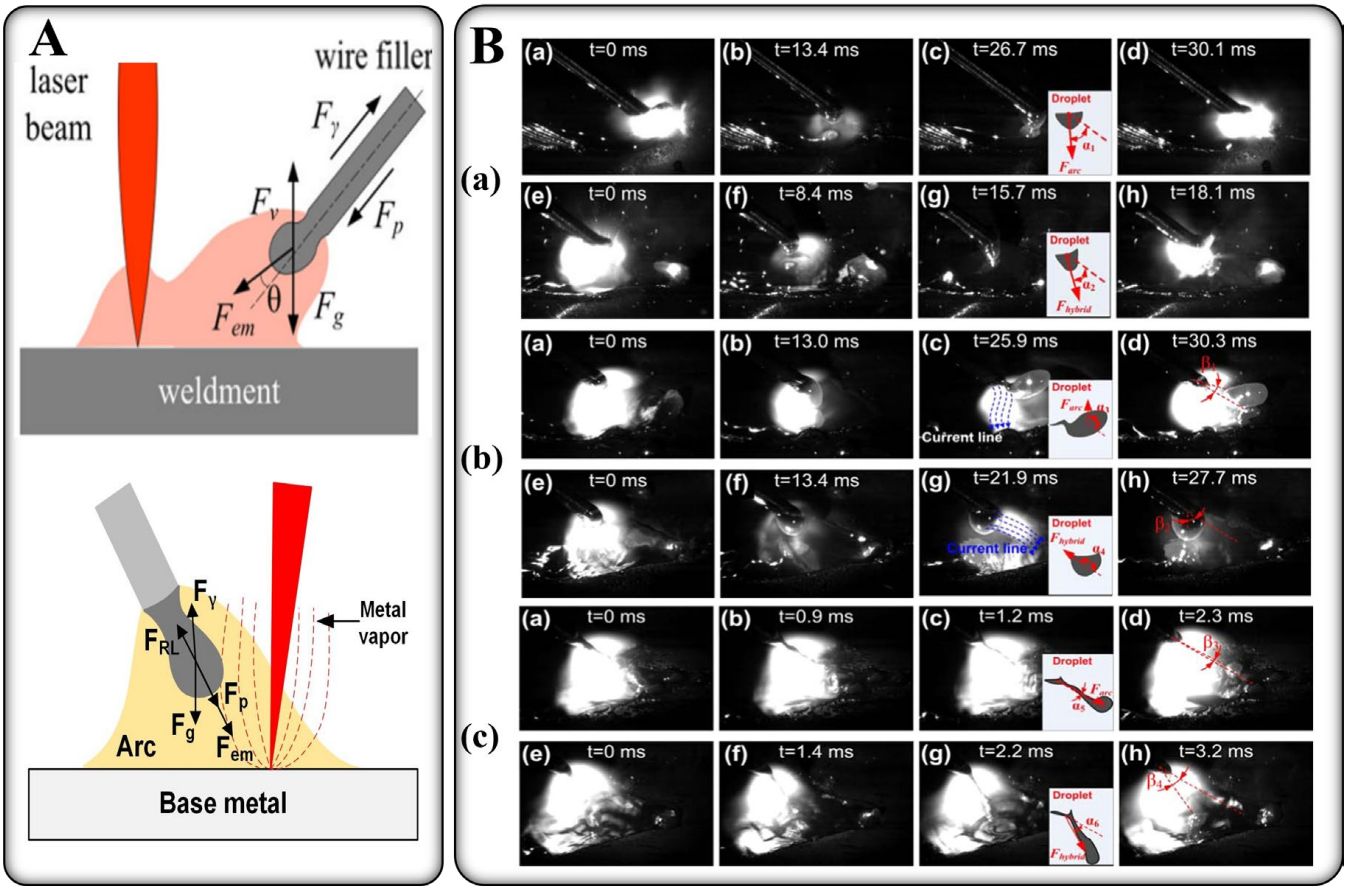


Figure 7. (**A**) Schematic diagrams of hybrid weld droplet forces (top) [91]. Reproduced with permission from SPRINGER NATURE; (bottom) [33]. Reproduced with permission from ELSEVIER. (**B**) Schematic diagrams of melt droplets' short-circuit transfer mode (**a**), spherical transfer mode (**b**), and spray transfer mode (**c**) processes in (**a**–**d**) conventional arc welding and (**e**–**h**) LAHW [115]. Reproduced with permission from ELSEVIER.

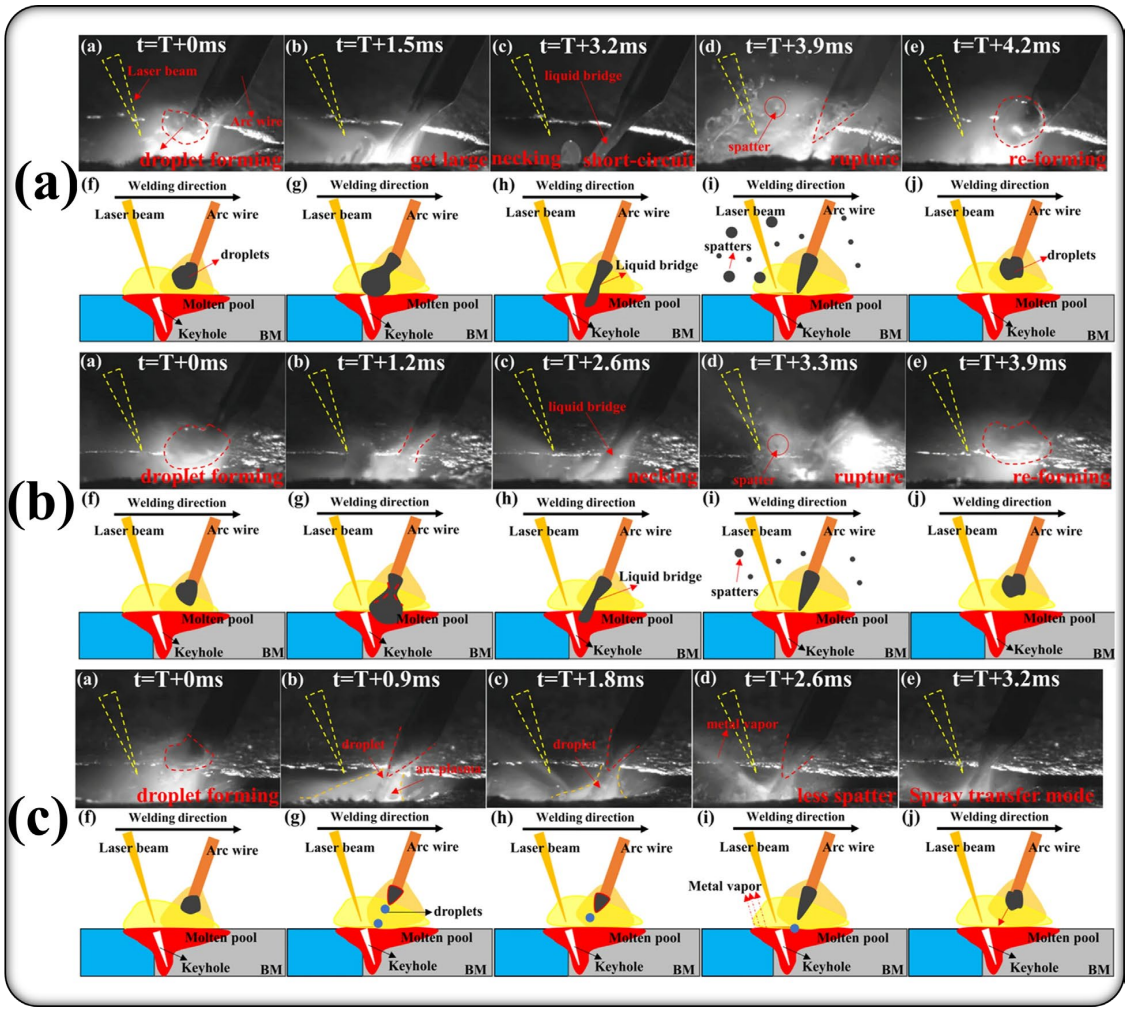


Figure 8. Samples of melt droplet transfer at different welding speeds, (**a**–**e**) are high-speed pictures of the droplet transfer at different times; (**f**–**j**) are diagrams corresponding to each moment [122]. Reproduced with permission from SPRINGER NATURE: (**a**) 3 m/min, droplet transfer mode is short-circuit transfer; (**b**) 4 m/min, droplet transfer mode is globular transfer; (**c**) 5 m/min, droplet transfer mode is spray transfer.

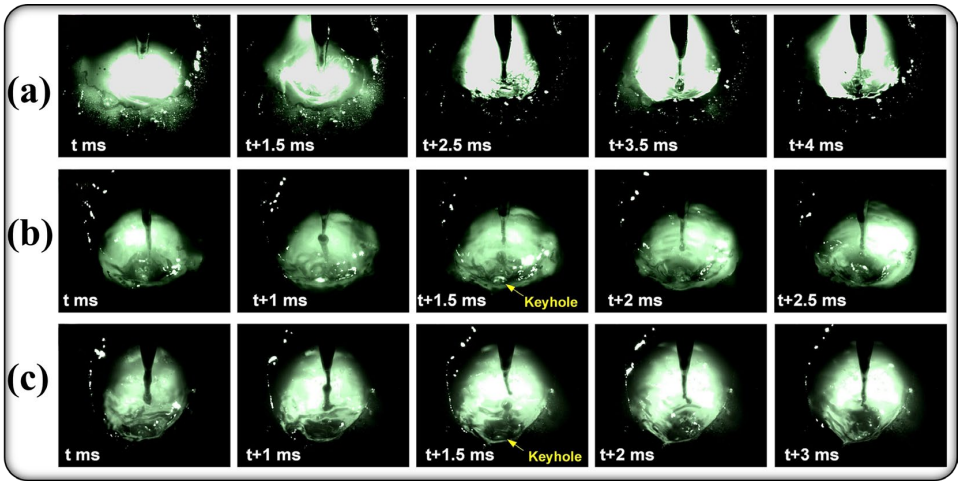


Figure 9. Schematic diagrams of melt droplet transfer processes at different laser powers [33]. Reproduced with permission from ELSEVIER: (**a**) 0 kW; (**b**) 3 kW; (**c**) 5 kW.

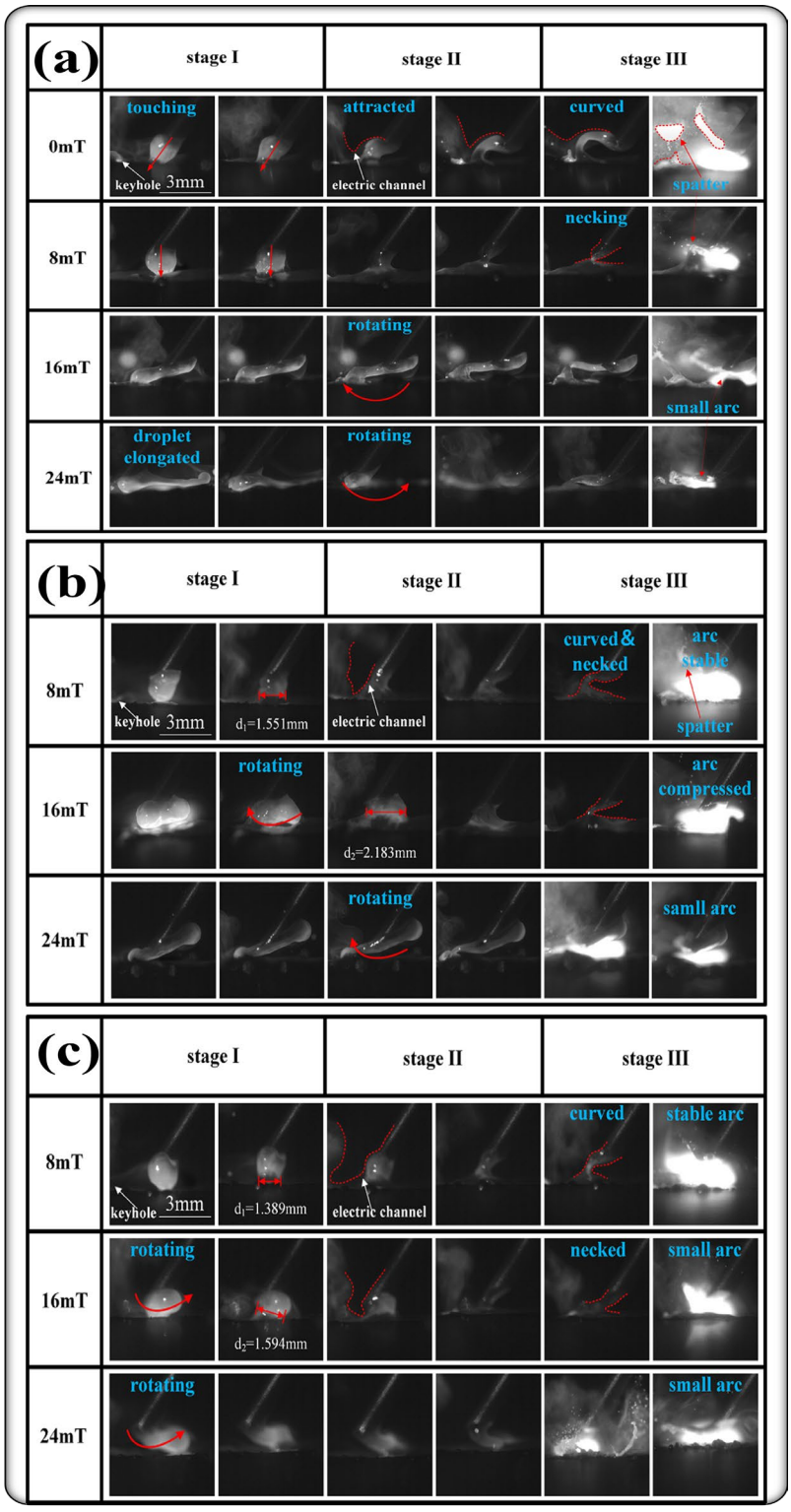


Figure 10. The droplet transfer process at different magnetic field strengths (8 mT, 16 mT, and 24 mT) and frequencies. Stage I represents the moment when the droplet contacts the molten pool and forms an effective liquid bridge. Stage II represents the bending of the liquid bridge. Stage III represents the breakage of the liquid bridge, forming the arc [123]. Reproduced with permission from ELSEVIER: (**a**) 0 Hz; (**b**) 10 Hz; (**c**) 20 Hz.

4.3. Weld Quality and Properties

The mechanical properties of weld seams are crucial indicators in welding engineering and significantly influence welding quality. Improved weld seam morphology

can enhance welding efficiency, stability, and the strength of welded connections, providing an intuitive representation of the advantages and disadvantages of the welding method [124,125]. Therefore, a primary focus in current welding processes is to identify strategies that produce welds with outstanding mechanical properties and minimal defects. A key approach for improving weld mechanical properties is by modifying the filler metal within the alloy, significantly enhancing the weld performance and meeting usage requirements [36,126–129]. Several factors influence the quality and shape of the final weld. This section evaluates weld quality and characteristics in hybrid welding by examining the residual stress, microstructure, composition, and various welding parameters to assess the benefits and features of the process.

4.3.1. Analysis of the Residual Stress

A successful weld requires addressing the residual tensile stress, which can arise from variable thicknesses, complex geometries, and erratic heat inputs. Residual stresses can degrade the mechanical strength of the weld, leading to reduced quality and performance, and an increased likelihood of cracking. Suppressing residual stresses is challenging, as welding involves frequent heating and cooling cycles. This process induces plastic deformation at elevated temperatures, causing expansion and contraction in both the FZ and base material (BM), leading to significant residual stresses and the deformation of the weld. Sun et al. found that increasing the heat input significantly raises the residual tensile stress in the weldment. The amplitude of the residual stress is generally determined by the heat energy input of the final weld bead, making residual stresses in the HAZ and at the base of the weld typically the highest [130]. Residual stress also arises from the mutual constraints between different regions at a local scale. In LAHW, the top of the welding flame is influenced by the arc's heat source, while the bottom is affected by the laser, which is more penetrating than the arc. The heat input, cooling rate, and weld metal vary in these areas, as do the amplitude and distribution of the residual stress. Ragavendran et al. analyzed the microstructural morphology and corresponding residual stress distribution resulting from thermal source effects in three different methods, as shown in Figure 11A. Compared to laser welding, both HLM and HLT produce distinct residual stress distributions, with a smaller heat-affected zone and lower residual stress in the weld region [131]. The influence of residual stresses on a weld is directly related to heat input and microstructural constraints, resulting in varying residual stress levels across different areas. These variations significantly affect the final shape of the weld. Figure 11B analyzes the longitudinal distribution of the residual stress along the plate thickness within the HAZ and across different weld regions from a three-dimensional perspective.

Finite element modeling (FEM) plays a crucial role in predicting residual stress during the LAHW process. This method simulates the distribution of heat sources during welding, as laser and arc thermal inputs exhibit distinct energy distribution characteristics. By modeling the temperature and stress distribution under the combined effect of the laser and arc, FEM can effectively assess the distribution of the residual stress and reduce the occurrence of defects [132]. The development of an appropriate heat source model is central to FEM analysis. Chen et al. proposed a novel "dual ellipsoid + conical" heat source model and applied it to the LAHW of 316L stainless steel, finding that this model accurately predicts residual stress induced by thermal input with a high level of precision [133]. Yang et al. employed a finite element model to calculate the LAHW joints of low-temperature high-manganese steel, and their results showed good agreement between the calculated residual stress and other parameters with experimental findings [134]. Hammad et al. developed a new 3D thermoelastic–plastic coupling model to predict residual stress and deformation in large ship structures because of LAHW. Their results

demonstrated that the model provided accurate predictions and revealed that the distribution of the residual stress is influenced by transverse and bending constraints [135]. Therefore, FEM offers the most effective and reliable method for predicting residual stress in LAHW joints, as it addresses the challenge of analyzing the correlation between stress fields and mechanical properties, thereby providing a theoretical basis for optimizing welding parameters.

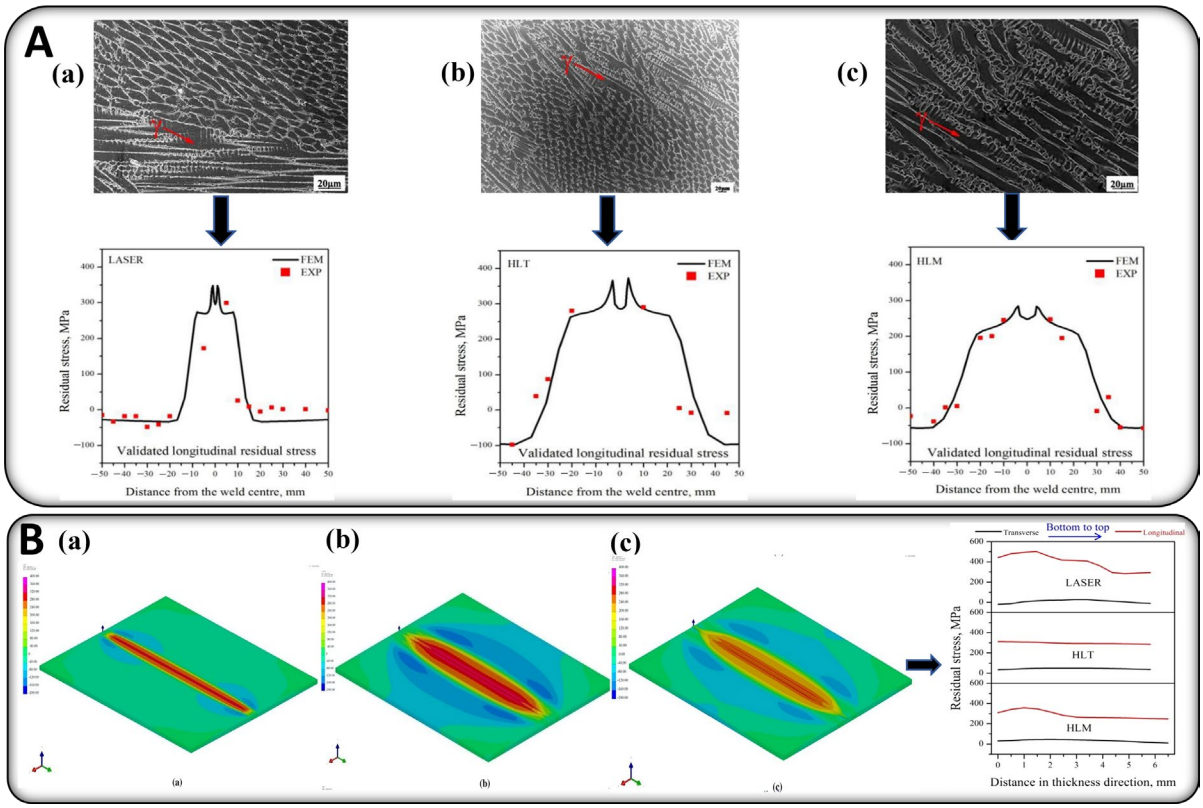


Figure 11. (**A**) Longitudinal residual stress distribution of welded joints obtained from microstructure measurements of welds for different welding methods, the red arrow represents the austenite in the tissue: (**a**) LW; (**b**) HLT; (**c**) HLM, [131]. Reproduced with permission from SPRINGER NATURE; (**B**) (**a**) LW; (**b**) HLT; (**c**) HLM welds' 3D residual stress distributions, with the right diagram showing the residual stress distribution along the thickness direction [131]. Reproduced with permission from SPRINGER NATURE.

4.3.2. Analysis of Microstructures

The microstructure plays a critical role in determining the mechanical performance of the welded area, including the organization and phase composition of the weld metal. The organization of the weld metal can be classified as equiaxial dendrites, dendrites, or columnar dendrites, depending on the specific alloys and welding conditions [136]. Equiaxial dendrites exhibit smaller grain sizes than columnar dendrites, contributing to the enhanced strength and mechanical properties of the weld [137,138]. The microstructural composition, resulting from various treatments, significantly affects the strength of the welded joint. Figure 12 presents microstructural images and the hardness distribution following hybrid welding and solution treatment, subsequently followed by aging (STA) in different regions. The results indicate that after the STA treatment, the distribution of the reinforcing phases and dislocations became more uniform, thereby enhancing the mechanical properties of the joint [46]. Schempp observed that high welding rates induce a transition in the solidification structure toward the equiaxial dendritic mode and that the use of grain refiners can further promote this transition [139]. Wang et al. proposed

laser oscillation as an effective technique for converting columnar dendrites to equiaxed dendrites, as the pulsating laser beam enhances the melt pool's flow and fluid dynamics. An increase in the dislocation density leads to a higher concentration of equiaxed dendrites, resulting in the improved mechanical strength of the weld [140].

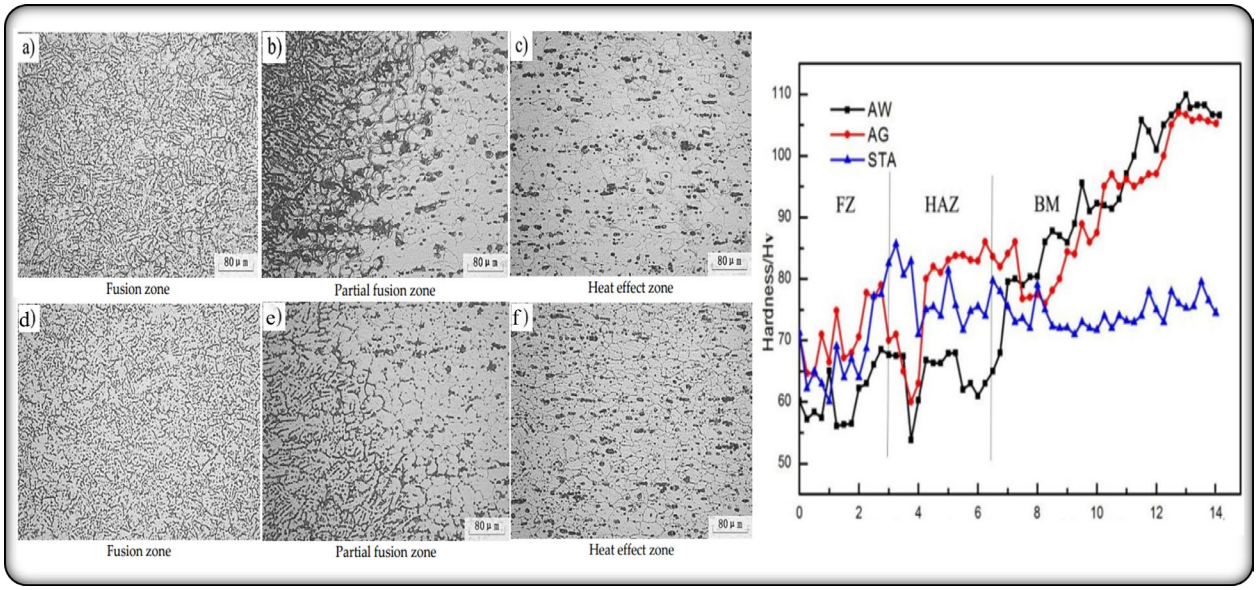


Figure 12. (**a**) The FZ of the hybrid weld, (**b**) the partial FZ, and (**c**) the HAZ; (**d**) the fusion zone after the STA treatment, with (**e**) the partial FZ and (**f**) the HAZ. The right figure shows the hardness distribution of the joints with different treatments, adapted from Ref. [46].

The phase composition significantly influences the mechanical strengths of welded joints. The formation of different phases in the weld affects its strength, hardness, and toughness, with both excessive and insufficient phase compositions reducing the weld's strength. Consequently, predicting and controlling phase compositions in advance can enhance the mechanical strengths of welds. Table 4 summarizes the phase structures and hardness values of hybrid welded joints for various materials, along with the factors contributing to the formation of these phase structures. In tensile experiments on hybrid-welded specimens, Du et al. discovered that the formation of martensite phases strengthens the FZ, improves the tensile strength, and enhances the strengthening effect of the fine grains. They also found that the samples were free from defects, such as fractures [141]. Chen et al. investigated the effects of the cooling rate on the microstructure and mechanical behavior of the HAZ in joints. Their findings indicate that the austenite–martensite mixture greatly affects both the quality and toughness of the joint. Inadequate control over this mixture may result in excessive martensite formation, which significantly enhances strength while simultaneously increasing the brittleness of the weld. Conversely, an insufficient amount of austenite fails to achieve the optimal balance between strength and toughness [142]. Additionally, the presence of the ferrite phase is associated with increased hardness in the weld. Ferrite is a strong phase characterized by a higher microhardness than austenite and a smaller heat-affected zone, typically located near the boundary of the fusion zone. Munro prepared HSLA-65 steel butt welds utilizing hybrid laser–arc welding. Upon evaluating the microstructure of each weld zone, it was found that acicular ferrite predominated as the primary component of the weld metal, contributing to enhanced strength and toughness [143]. Acicular ferrite is a critical microstructural component that improves the performance of low-carbon-steel weld joints. Zhang et al. developed a smoothly transitioned weld layer by fusing 40 mm thick mild steel using hybrid welding techniques. Their findings indicate that the weld seam area exhibits characteristics of

the root layer, filler layer, and overlapping interlayer, as shown in panels (a) and (b) of Figure 13A. The tensile strengths at various locations within the weld were subsequently evaluated, and an EDS analysis of the weld's composition was performed, as shown in Figure 13A, panels (c–f). This analysis revealed that the bottom specimen of the root laser zone had a low acicular ferrite fraction and the lowest mechanical strength, which was attributed to rapid cooling. Therefore, acicular ferrite plays a crucial role in improving the performance of low-carbon-steel joints [144]. Overall, key microstructural features, such as grain size and phase composition, significantly affect the mechanical properties of welded joints. Fine grains enhance strength and toughness by obstructing dislocation movement. The phase composition, including martensite and ferrite, influences the weld's strength and hardness. For instance, acicular ferrite significantly improves both strength and toughness, particularly in low-carbon steels [143,144]. Additionally, second-phase particles can enhance fatigue strength. Therefore, the precise control of welding parameters to regulate these microstructural features can effectively optimize the mechanical performance of welded joints.

Table 4. Phase microstructure and hardness in regions of different materials in hybrid welding.

Material	Phase Formation Region	Main Phase Structure	Organization Formation Mechanism	Micro-Hardness (Hv)	Ref.
Chromium–molybdenum alloy steel plate	FZ	Martensite	The FZ of chromium–molybdenum alloy steel undergoes the transformation from austenite to martensite under rapid cooling conditions, resulting in a significant increase in hardness.	≈ 400	[141]
High-strength low-carbon bainitic steel	HAZ	Martensite–Austenite	A moderate cooling rate in the HAZ causes a part of the austenite to transform to martensite, while the remaining portion forms a martensite–austenite mixed structure.	284 ∼ 298	[142]
High-strength low-alloy (HSLA-65) steel	FZ	Acicular ferrite	The formation of acicular ferrite is associated with a lower carbon equivalent and a lower cooling rate. Rapid cooling promotes the formation of ferrite while suppressing the generation of martensite and bainite, thereby enhancing the toughness of the joint.	257 ∼ 277	[143]
40 mm thick hot-rolled annealed Q235 low-carbon steel	FZ	Acicular ferrite	The rapid cooling rate at the root FZ, along with the alloy composition (Mn and Si), promotes acicular ferrite formation, enhancing the weld strength and toughness.	≈ 280	[144]
316L stainless-steel plate	HAZ	Ferrite	The high Cr and Ni contents in 316L stainless steel enhance the ferrite's stability, while slower cooling facilitates its stable precipitation in the HAZ, thereby improving the weld joint's stability and corrosion resistance.	191.1 ∼ 195.4	[145]

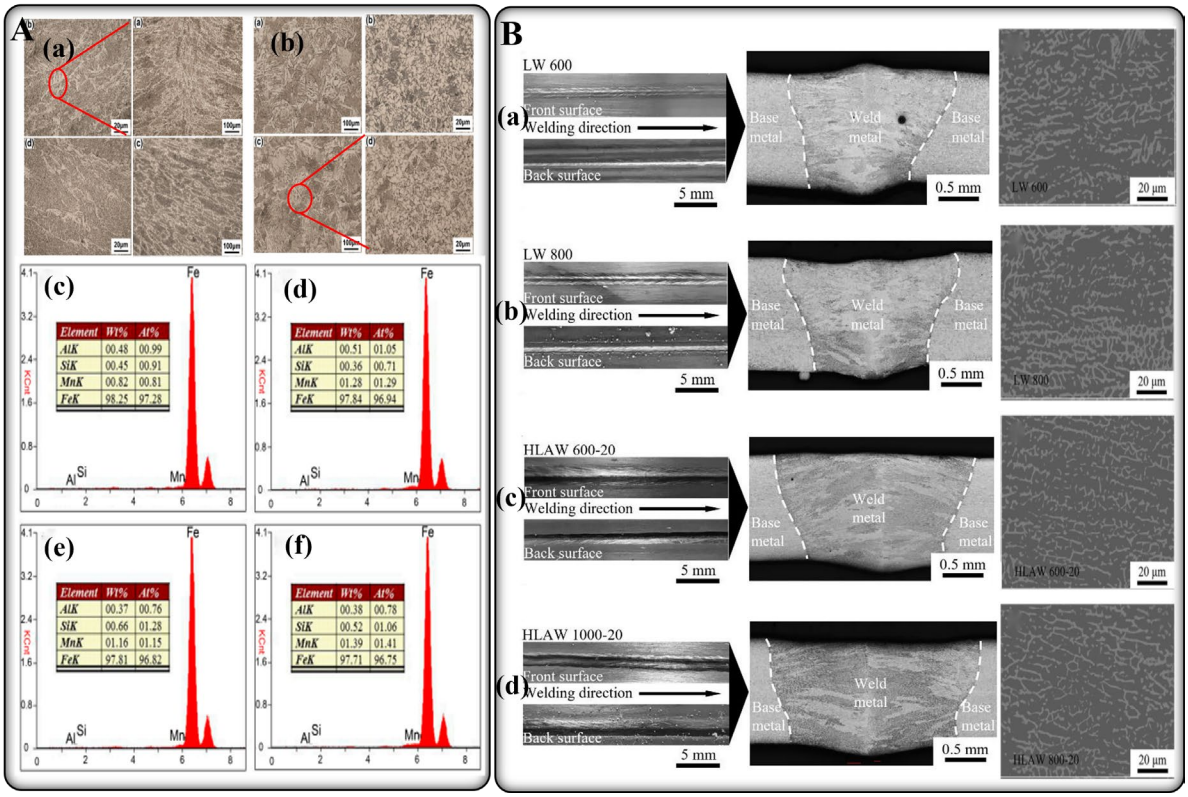


Figure 13. (**A**) Root layer microstructure (**a**) and filler and overlapping interlayer microstructure (**b**). (**c**–**f**) The phase composition from the EDS analyses of different regions within the weld seam, adapted from Ref. [144]; (**B**) surface morphologies and cross-sectional appearances of welds: panels (**a** ,**b**) represent laser welding, while (**c**,**d**) depict hybrid welding. Surface shapes and cross-sectional morphologies of welds for different welding methods (on the **left**); microstructural images of the weld material, as viewed under an optical microscope (on the **right**), adapted from Ref. [145].

The microstructure and phase composition are temperature dependent, as reflected in variations in the grain size and phase organization. The heat input promotes grain growth and changes in the organization of the weld region while also influencing the depth of the fusion, weld properties, and overall microstructure. Establishing a connection between the heat input and local microstructure facilitates further investigation of the weld region. Welded joints have regions, like the HAZ and the FZ. The mechanical strength of the weld material improves as its grain size decreases. The grain size is directly affected by the heat input during the welding process. Excessively high temperatures lead to increased heat input, causing rapid grain growth. Shen et al. discovered that reducing the heat input results in the formation of smaller grain structures, which enhance the mechanical strength of the formed layer [146]. Consequently, as the heat input increases, the grain size of the weldment also increases, resulting in a reduction in the weld quality and an increase in the weld distortion. Ragavendran and Vasudevan et al. created 316L-type welded joints with HLM and HLT and conducted a thermodynamic analysis. They discovered that an increase in the heat input leads to an expansion in the volume of the weld metal. The amount of the heat input and the shape of the weld metal significantly impact the maximum residual tensile stress in the weld and its distribution [131]. To minimize grain growth during welding and mitigate distortion caused by heat, it is recommended to increase the laser-to-arc-energy ratio while simultaneously decreasing the heat input [146–149].

The inherent advantages of LAHW technology enhance the weld quality by regulating the heat input and improving the weld microstructure. Jiang et al. investigated MIG

welding with HLM and discovered that laser hybrid welding causes significantly less distortion than regular MIG welding. This is because of the rapid welding speed of LAHW, which minimizes excessive heat input and, thus, reduces the risk of welding deformation [75]. Xie et al. conducted a comparative analysis of LW and LAHW and found that for identical welding parameters, the energy input in LAHW is less concentrated because of the influence of the arc. This results in finer grains and the enhanced mechanical strength of the welded connection. As shown in (c) and (d) of Figure 13B, the weld bead produced using LAHW is significantly smoother compared to the one produced using LW, indicating a more refined weld surface. [145]. In summary, the quality and mechanical strength of welded connections depend on the type of filler material used and the resulting microstructure. In LAHW, the weld structure is more complex than those in traditional welding approaches because of the interplay among various parameters. Therefore, it is essential to control the influence of the weld microstructure, along with the welding parameters and heat input, to achieve the optimal weld morphology.

4.3.3. Analysis of the Influences of the Welding Parameters

The selection of the welding parameters significantly influences the weld quality [150]. The introduction of shielding gas is a crucial aspect of pre-welding preparation. The stability and heat distribution of the weld are influenced by the composition and volume fractions of shielding gases, which, in turn, affect the weld penetration and stability. Optimizing the shielding gas characteristics can enhance the weld quality and reduce flaws, such as porosity [151]. Noble gases, such as helium (He) and argon (Ar), are commonly used to shield the molten pool from the environment. He, which has a high ionization potential, reduces the density of the plasma, thereby narrowing the arc and enhancing the depth of the fusion during welding. However, its lightweight nature makes it less stable than heavier, more easily shielded gases. The lightness of He compromises its stability compared to that of the heavier and more ionizable argon [152,153], and it demonstrates poor performance when used independently. Tani et al. utilized a gas mixture containing 30% to 40% helium as a shielding gas in a LAHW process that combines a CO_2 laser and MIG. They noted a favorable process feasibility; however, they discovered that using too much He might result in an unstable welding process. Therefore, managing the proportions of shielding gases presents a challenge [154]. Ahn et al. studied the impact of an Ar-He shielding gas mixture on the weld seam quality. They found that adding He to the weld seams increases the heat input, raising molten pool temperatures and extending cooling and solidification times. Prolonged cooling and solidification negatively affect the weld quality by allowing bubbles to dissipate fully, thereby reducing porosity. Additionally, the shielding gas creates a stable environment that prevents the oxidation or contamination of the molten pool and metal at high temperatures [155].

In addition to He and Ar shielding gases, several studies have demonstrated significant variations in the effects of alternative gas mixtures on the weld seam quality. Wallerstein et al. found that using Ar + 8% CO_2 and Ar + 15% CO_2 as shielding gases resulted in the greatest penetration depth and highest-quality welded junctions. They also found that adding CO_2 increases the wettability of the molten metal, minimizes film formation in the weld region, and prevents dents and flaws [156]. Fang et al. found that the welding stability improves when Ar + CO_2 is used as a shielding gas. Additionally, the weld's mechanical strength can be improved, and the grain size reduced, by appropriately adding nitrogen to the shielding gas. However, the average hardness of the weld decreases if too much nitrogen is added [157]. Bai et al. discovered that adding 5% CO_2 or nitrogen to the shielding gas can prevent the oxidation of the hybrid welded seam, hence improving the weld's performance [158]. Yang et al. employed CFD and high-speed photography to

analyze how the shielding gas flow rate influences the LAHW welding process. They found that a suitable shielding gas flow rate effectively prevents the oxidation of the weld, resulting in a superior appearance [159]. Consequently, the use of shielding gases emerges as a critical factor in producing high-quality welds. To ensure welding quality and efficiency, simulating and analyzing gas composition in various welding processes is essential.

In addition to the shielding gas filler and its composition, parameters, such as the laser power, influence the weld depth and joint defects. Table 5 presents the mechanical properties of LAHW joints fabricated under various welding conditions. Ragavendran demonstrated that sufficient laser power is required to form a stable, well-shaped keyhole for the desired penetration depth in high-quality welds. Excessively high power can lead to defects and residual stresses [131]. Chen et al. investigated the effects of the laser power on weld formation. A satisfactory weld is achieved with a 1.5 kW laser power, although the weld lacks noticeable hybrid welding characteristics. When the laser power is increased to 2.5 kW, the weld penetration improves visibly. However, the intense interaction between the photoplasma and arc plasma impairs the welding stability and filler metal quantity, reducing the weld's reinforcement [160]. Additionally, the position of the laser focus is crucial for determining the weld penetration, with the optimal penetration occurring when the focal point is just below the workpiece's surface [151]. The arc angle also influences the weld penetration, as the arc electrode's size affects the deflection of the shielding gas against the laser-induced plasma, thus impacting the laser's penetration of the weld [161]. Therefore, achieving high-quality welds with LAHW requires the simultaneous adjustment of multiple welding parameters to ensure the optimal morphology.

Table 5. Mechanical properties of the optimal LAHW joints fabricated under different conditions (welding speed, laser power, and shielding gas composition).

Material	Process	Shielding Gas	Welding Speed ($mm \cdot s^{-1}$)	Laser Power (KW)	Tensile Strength (MPa) Hardness (HV)	Ref.
08Cr19Mn6Ni3Cu2N stainless-steel plate	Hybrid laser–MIG welding	95%Ar + 5%CO_2	7.5	3.6	MPa = 714	[157]
High-nitrogen austenitic stainless steel	Hybrid laser–MIG/MAG arc welding	90%Ar + 5%N_2	11.6	2.2	HV = 270~390	[158]
Non-heat-treated forged aluminum alloy(5083-O)	Hybrid laser–MIG welding	100% Ar	30.0	2.5	MPa = 74~97	[28]
AISI 316L(N) SS	Hybrid laser–MIG welding	99.999% He	16.6	2.5	HV = 155~215	[131]
SA516 grade 70 steel	Hybrid laser–MIG welding	99.999% Ar	16.6	2.0	HV = 195~465	[77]
ASTM A1066/A1066M	LAHW	80% Ar + 20% CO_2	2.6	4.8	MPa = 817 HV = 250~325	[142]

Oscillating laser–arc hybrid welding (O-LAHW) offers several advantages, including improved weld shape, defect suppression, and grain refinement. The oscillating laser beam intensifies the stirring effect within the molten pool, promotes energy distribution, and regulates the weld width, thereby mitigating defects, such as porosity and concave edges [162]. Introducing an oscillating laser beam modifies the energy input, broadening the laser energy distribution, which, in turn, increases the weld width and decreases the weld depth. This modification ensures the complete escape of bubbles. Wu et al. manipulated the oscillation magnitude and evaluated the welding process stability by measuring the standard deviation of the current and voltage. They found that the welding stability improved when the oscillation amplitude was maintained between 0 and 3 mm.

Furthermore, it was observed that the transition between different passes was smooth, resulting in a weld that was nearly free of defects [163]. Shi et al. reported that increasing the oscillation frequency of the laser led to a reduction in the depth of the molten pool's keyholes, making the molten pool shallower. This reduction resulted in decreased weld porosity, ultimately eliminating it. Moreover, the oscillating laser beam creates a vortex in the opposite direction, enhancing both the temperature field and energy distribution within the molten pool. Therefore, applying O-LAHW enhances the process stability, reduces defect occurrence, and produces superior weld quality [164].

4.4. Welding Defects and Suppression

The synergistic effect of heat sources in LAHW complicates the process. For example, the preheating effect of the arc increases the material's ability to absorb laser energy, but it also accelerates material evaporation, resulting in greater instability. The combination of heat sources requires adjustments to multiple parameters, which are closely related to the formation of weld defects. This is particularly relevant as neither welding method imposes additional speed restrictions. When these two welding methods are combined, low arc-welding speeds reduce the effectiveness of laser-induced deep-melt welding, while excessively high speeds can destabilize the arc. Consequently, welding defects are exacerbated by these factors [165]. Pores, a severe welding defect, can negatively impact the mechanical properties of the weld by reducing its effective working area and causing stress concentration [166]. Other defects, such as cracks, humps, and biting edges, directly impair the weld quality. Previous studies have investigated various methods for predicting defects in LAHW, including high-speed imaging and digital non-destructive testing, which are effective in detecting the formation and evolution of keyholes and other defects. Common strategies for mitigating defects involve adjusting process parameters, among other techniques [167].

4.4.1. Porosity Defects

Porosity in hybrid welding primarily arises from the collapse of keyholes formed by the laser beam. The weld porosity significantly reduces the tensile strength of the weld metal, making it a critical concern in welding. Uneven stresses on the keyholes lead to considerable variations in their shape and size, resulting in the formation of numerous bubbles at the bottom. As these keyholes collapse, the bubbles rise. During weld solidification, if the heat source generates a narrow molten pool, most of the bubbles will become trapped within the weld, forming pores. Therefore, a feasible approach to reduce porosity is to enhance the keyhole stability and create a broader melt pool. In LAHW, the addition of the arc mitigates the temperature gradient during welding, increases the molten pool's area, and prolongs the solidification time. This results in reduced porosity compared to that achieved using individual welding methods, as it allows the bubbles to escape from the molten pool [168].

The stability of the keyholes is primarily influenced by several welding parameters, including the welding speed, arc energy, laser power, and shielding gas. By regulating these parameters, the stability of the keyholes can be effectively enhanced, thereby minimizing the formation of porosity. As illustrated in Figure 14A, an increase in the laser power leads to a higher porosity, while an increase in the arc current reduces the porosity. Notably, the increase in the welding speed (from 1 m/min to 1.5 m/min) significantly increases the porosity. Cai et al. investigated pore defects during the HLM of aluminum alloys with pure Ar and varying He volumetric ratios. Their findings revealed that He shielding gas with a volumetric ratio of 50% increased the stability of the locked pores and produced the greatest reduction in the porosity [169]. Panwisawas et al. used CFD simulations to study the formation of keyholes and porosity, finding that a high welding speed could produce

a narrow fusion zone and increase the keyhole stability, thus reducing the likelihood of pore formation. They also noted that smaller plate thicknesses effectively reduced porosity during welding [170]. Vorontsov et al. observed a significant increase in porosity at low welding rates after applying LAHW to the alloy AA5083. At high speeds, the porosity of the resulting welds was as low as 0.07%; however, it was also observed that when the welding speed was excessively high, specifically between 6.5 m/min and 7 m/min, welding defects became more pronounced, adversely affecting both the weld quality and microstructure [171]. Miao et al. reported that an increase in the welding speed resulted in a reduction in the molten pool's height, a shortening of the bubbles' escape path, and a decrease in porosity. They found that as the welding speed increased, the porosity was significantly suppressed, decreasing from 13% to 5% [172]. Yan et al. discovered that increasing the arc current or reducing the laser power, in their investigation of the porosities and microstructures of hybrid welded joints, minimized the keyholes' aspect ratio, enhanced stability, and reduced bubble formation [173]. Leo et al. demonstrated that the arc's power effectively inhibits porosity proliferation in weldments. Furthermore, the weld performance improves as the ratio of the arc's power to the laser's power increases. They observed that excessive laser power causes metal evaporation, leading to a significant increase in the porosity [174,175]. Given the complexity of hybrid welding, it is essential to consider multiple factors. Therefore, the optimal strategy for reducing porosity involves controlling welding parameters to improve the keyhole stability.

4.4.2. Crack Defects

Cracks are a common defect observed in LAHW. The formation of cracks in the weld area can significantly impact the stability and quality of the welded structure [125]. The occurrence of these cracks is linked to fluid convection caused by temperature disparities during the solidification process. Variations in the metal's viscosity during solidification lead to deformation and the development of tensile strains within the solid metal. As the temperature difference increases, differential thermal contraction results in significant localized deformation. Cracks form when this distortion exceeds the ductility of the weldment and when no filler metal is present [23]. In Figure 14B, panels (a) and (b) illustrate the morphology of the crack initiation regions, while panels (c) and (d) show the subsequent zones of the stable crack propagation. Furthermore, the welding process generates residual stresses that further facilitate crack propagation, as shown in Figure 14B, panels (e) and (f). The formation of cracks is associated with excessive cooling rates, and some welding defects may appear concurrently with cracks. The shape of the crack is influenced by the temperature distribution along the welding direction, which creates transverse stresses within the weld during the cooling phase, potentially leading to the formation of transverse cracks. Hagenlocher discovered that transverse fractures act as initiation points for longitudinal cracks, significantly increasing the extent of cracking in the weld [176].

Cracks significantly diminish the overall performance of welds. Zhang et al. utilized LAHW to treat copper–aluminum alloys and observed that the tensile specimens exhibited a notable presence of microcracks, which led to a decrease in the overall tensile strength [125]. Consequently, they concluded that the weld's quality depends on both microcracks and macrocracks. Chen et al. conducted a study to analyze the impact of the cooling rate in LAHW on the structure of the HAZ. They discovered that higher proportions of martensite and bainite increase the susceptibility of this zone to stress concentration, resulting in crack formation. As these components' contents increase, the occurrence of fractures also rises, including the formation of microcracks, which ultimately leads to a decrease in the material's toughness [142]. Prior research has indicated that the occurrence of cracks can be

minimized by employing optimized welding parameters or by incorporating filler wires with a high silicon content [148]. However, the wider heat-affected zone of the hybrid weld itself reduces stresses compared to laser welding, thereby somewhat suppressing crack defects. In addition to controlling welding parameters, extensive research has demonstrated that the use of filler materials with high silicon contents enhances weld ductility while effectively reducing the risk of crack formation [177,178]. Consequently, the selection of suitable filler materials and the application of appropriate heat treatments can significantly reduce residual stresses and mitigate the occurrence of cracks.

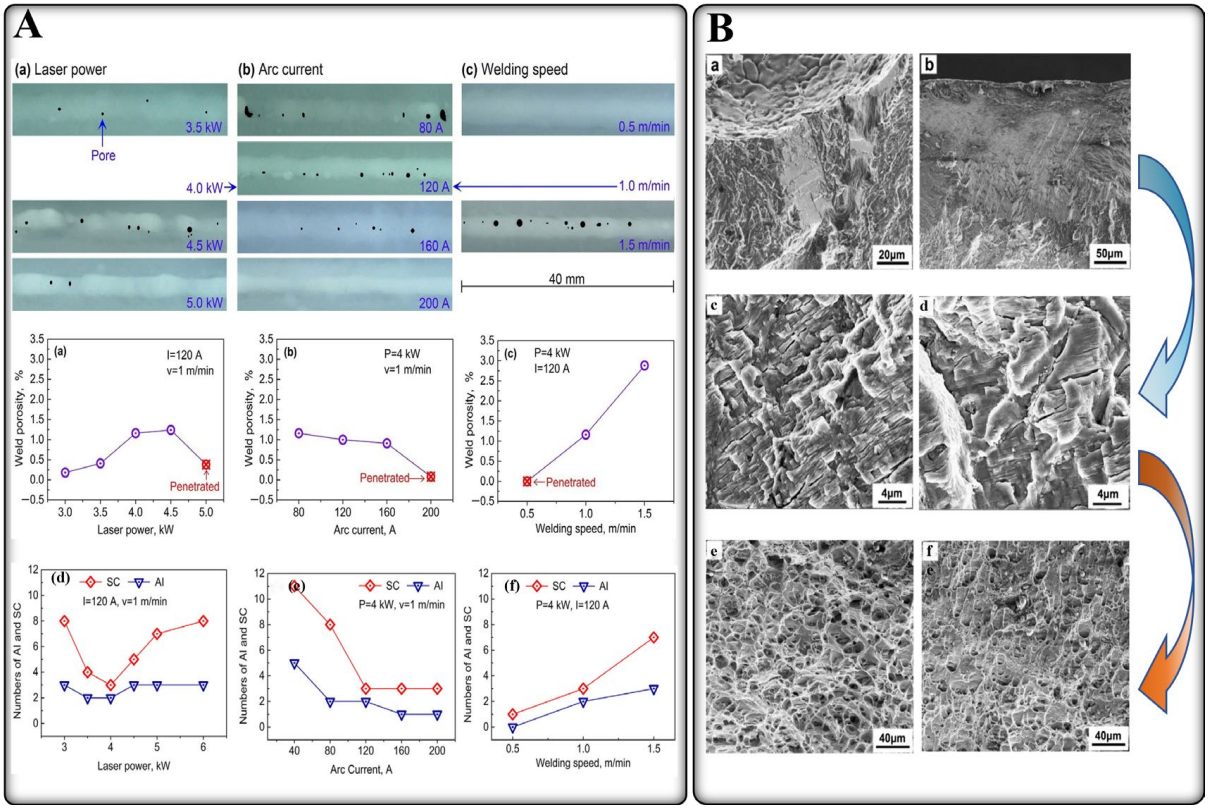


Figure 14. (**A**) Effects of different parameters on porosity (**upper** panel) and stability (**lower** panel): (**a**) laser power, (**b**) arc current, and (**c**) welding speed, adapted from Ref. [179]; (**B**) Schematic diagram of welded joint cracks, adapted from Ref. [148]: (**a**,**b**) represent the crack initiation zones; (**c**,**d**) represent the stable crack growth zones. The final crack morphologies: (**e**) the final equiaxed ductile dimples and (**f**) U-shaped ductile dimples.

4.4.3. Hump Defects

High welding speeds, high laser powers, and enhanced gap-bridging capabilities are advantages of LAHW; however, they also exacerbate the formation of humps. Under the effect of the surface tension, the flowing melt is obstructed by the prematurely solidified molten pool, leading to a build-up of material. This accumulation, through repeated cycles, results in the formation of a hump [180]. Tang et al. investigated the process of hump development and showed, using a molten pool diagram, that the major causes of hump formation are the surface tension and pool weight, with hump formation being inhibited by increasing the weight of the molten pool [180]. Xue and colleagues employed mathematical modeling to examine how the surface tension influences the development of humps. They applied a TIG arc after lasering and discovered that the arc's activity made the molten pool widen and level. Moreover, the TIG arc prevented the melt from flowing at a high rate of speed throughout the operation, which lessened the instability and suppressed hump

formation [181]. Low welding speeds and laser powers were also found by Bunaziv et al. to be efficient in suppressing hump formation in the laser–arc single-pass welding of materials ranging in thickness from 12 mm to 15 mm [182]. In summary, various perspectives, including the surface tension, molten pool weight, arc effects, and heat input, have been proposed to support different theories of hump formation. However, none of these theories fully integrates all the parameters that influence the molten pool. Therefore, to gain a comprehensive understanding of the primary causes of hump formation, it is essential to develop a model that incorporates all these factors, thereby providing a more accurate prediction of and an effective approach for mitigating this defect type.

5. Industrial Applications

The demand for hybrid welding in industry is increasing because of its significant advantages. This welding technique can lead to cost savings by reducing both the time required for welding and the amount of materials utilized [183]. Practical applications can achieve further cost reductions by employing a 3 kW laser instead of a 4 kW laser, which results in lower investment costs [184]. The first industrial implementation of LAHW was successfully achieved with the introduction of the pioneering HLM system by Fraunhofer ILT in Germany, specifically at an oil pipe manufacturing company. This innovation has transformed the welding industry. Its substantial cost and industrial benefits have enabled major sectors, such as automotive [185], shipbuilding [186,187], pipeline transmission [188], and aerospace [189], to adopt this technology in their operations. However, this technology still faces significant challenges, including high investment costs and the complexity of integrating different heat sources, which limit its widespread adoption. Laser-assisted hybrid welding has been successfully applied in industries such as automotive and shipbuilding because of their demand for advanced welding technologies, with long-term cost savings justifying its use [190]. Traditional welding techniques, such as tungsten–inert gas (TIG) and metal–inert gas (MIG), often have lower initial investment costs and simpler integration, making them more accessible for small and medium-sized enterprises. However, these traditional methods generally result in longer welding times and higher material usage, leading to increased operational costs over time. In contrast, LAHW's advanced capabilities enable faster welding and more efficient material usage, offering long-term savings that can offset its initial high costs. Additionally, the complexities of heat source integration require specialized training and maintenance, which increase operational costs and limit LAHW's application in non-critical industries. Despite these challenges, LAHW remains a transformative technology, and further research into cost-effective solutions could accelerate its adoption and enhance its industrial applicability.

5.1. Applications in the Automotive Industry

A significant portion of the welding processes in automobile manufacturing involves the use of LAHW for component fabrication. Given the diverse welds with varying structural and morphological requirements in automobile production, hybrid welded joints facilitate a more effective joining of different plate types and thicknesses. These joints provide advantages such as increased welding speeds, reduced energy input, and minimized distortion. Volkswagen and Audi exemplify these applications, as both companies employ laser–MIG hybrid welding in their automotive manufacturing lines to produce vehicles [185]. Staufer noted that even at elevated welding rates, hybrid welds maintain a satisfactory depth of fusion in automobile manufacturing, particularly for axles [184].

5.2. Applications in the Shipbuilding Industry

To significantly enhance productivity and production capacity, shipbuilders have increasingly adopted laser–arc hybrid welding across numerous production lines. This shift is driven by the substantial quantities of 8 to 20 mm thick steel required for decking in shipbuilding. Consequently, metal products are more susceptible to considerable weld distortions caused by high heat input and thermal cutting, which can adversely impact productivity because of the necessity for correction and adjustment work. In contrast, laser–arc hybrid welding can directly mitigate the hazards associated with heat distortion. Meyer–Werft in Germany was the first shipbuilder to implement laser–arc hybrid welding in its production line. They utilized a combination of CO_2 laser and MIG arc to weld ship plates, resulting in significant time savings in shipbuilding while simultaneously reducing weld distortion. Since then, this welding method has garnered increasing attention at commercial shipyards. Hiroshi reported that the hybrid welding technique is suitable for general merchant vessels, including crude oil carriers, container ships, and cryogenic carriers. LAHW has been employed in the superstructure of the hull and in the thinner steel plates of the nacelle [191]. Uemura utilized a manipulator to examine the suitability of LAHW in both horizontal and vertical positions, concluding that LAHW is also appropriate for large steel welding at shipyards [192]. Subsequently, LAHW has been adopted by Kvaerner in Finland and Fincantieri in Italy. Kristensen has indicated that at least 20% of the shipbuilding person–hours are allocated to rework because of weld distortion [193]. Laser–arc hybrid welding addresses this issue by modifying the shape of the weld, eliminating concave edges and reducing the propensity for cracking.

5.3. Applications in the Aerospace Industry

Titanium alloys and aluminum alloys are the primary materials utilized in aeronautical construction [21]. In airplane construction, LAHW is frequently employed to weld thin titanium and aluminum alloy panels. The reinforced aluminum alloy AA7075 is commonly used in airplane manufacturing. Ola applied hybrid welding to AA7075-T651 and noted that there were no fractures in the weld and that solidification cracking was absent from the fusion zone. A simultaneous comparison with laser welding demonstrated that hybrid welding exhibited significant advantages [194]. The AA6013 alloy possesses a very high damage tolerance, making it an excellent choice for airframe applications. It was observed that the welds remained intact, free of porosity, and exhibited very few surface flaws when CO_2 and Nd:YAG lasers were utilized for LAHW in conjunction with MIG arc welding [195]. The 5083-aluminum alloy is known for its exceptional corrosion resistance. Huang implemented a hybrid welding technique using laser–arc welding on the 5083 aluminum alloy, finding the process to be highly stable and yielding a weld with very low porosity [27].

5.4. Application of Hybrid Welding Technology in Additive Manufacturing

Laser–arc hybrid additive manufacturing (LAHM) technology offers higher power density and more precise arc control compared to those of wire arc additive manufacturing (WAAM). It effectively manages the local high-temperature heat-affected zone during the additive process, stabilizing the molten pool shape and size, thereby improving the surface precision, forming quality, and deposition efficiency [196–198]. In the fabrication of aluminum alloy thin-walled parts, LAHM exhibits superior tensile strength and microhardness compared to those achieved using WAAM, meeting the strength requirements for thin-walled components [199]. In copper alloy additive manufacturing, laser–arc hybrid welding effectively overcomes the high reflectivity issue encountered in laser additive manufacturing, significantly enhancing both the quality and efficiency of copper alloy

deposition [200]. For rare metal additive manufacturing, oscillated laser–arc hybrid additive manufacturing has substantially improved the tensile strength of arc-deposited materials [201,202]. The research on laser–arc hybrid additive manufacturing demonstrates that this technology significantly enhances the precision and efficiency limitations of WAAM while improving the ability to fabricate high-performance materials. As a result, LAHM holds promising prospects for industrial applications in the aerospace, automotive, energy, and medical sectors. However, to achieve a broader range industrial applications, LAHM technology must address the complexities of process control that the combination of heat sources may introduce when dealing with high-performance alloys, requiring accurate predictions to ensure the optimal deposition quality.

6. Conclusions and Outlook

This work presents a comprehensive assessment of the current advanced welding technology of LAHW. The existing technology and research have demonstrated the unique advantages and performance of this method, wherein the synergistic effect of the heat sources addresses common challenges encountered in the individual welding processes. Compared to AW, hybrid welding can increase weld speeds without compromising weld quality, while the heat input can be precisely controlled to mitigate high residual stresses in the weldment, thus reducing the rework time associated with thermal distortion. In comparison to laser welding, hybrid welding provides superior gap capabilities and can achieve high welding speeds and deep melting capacities characteristic of LW. The principle of the heat source synergy in hybrid welding is elucidated through the plasma interaction effect of the two heat sources. The extent to which the laser and arc can produce a synergistic effect depends on the regulation of parameters and the arrangement and combination of the laser and arc. This is summarized in the contexts of the keyhole behavior and different droplet transition modes in hybrid welding. Keyhole stability has been extensively documented in the literature as a crucial prerequisite for the formation of high-quality welds. However, the unique heat-source-coupling mode of LAHW results in keyhole stability that is significantly poorer than that of single LW. An analysis of the reasons for this reduced stability reveals that the modulation of the parameters and the applied environment can enhance keyhole stability. This study specifically investigates the residual stresses in hybrid welding and methods for their prediction and suppression, as well as the impacts of the microstructure and welding parameters on the mechanical properties of the weld. Additionally, it was found that an oscillating laser–arc hybrid welding method effectively addresses the issue of weld deformation. This study enumerates welding defects, such as porosity, cracks, and humps, and provides an analysis of their formation and suppression.

LAHW is gaining industrial popularity and has been widely adopted in the automotive and shipbuilding industries, as well as by aerospace companies, pipeline transportation companies, power generation firms, and manufacturers of on-road heavy-duty vehicles, among others. These applications have demonstrated their potential for commercial use. In the automotive sector, this technology enables a more seamless joining of plates of varying thicknesses while minimizing deformation. However, as lightweight vehicles become increasingly prevalent, the requirements for thin plate welding, particularly regarding arc power, will intensify. Current hybrid welding methods have not yet achieved significant breakthroughs in this area, indicating a need for advancements. In the treatment of medium-thick plates, commonly utilized in shipbuilding, this technology can reduce the rework time and enhance the quality of weld seams. In the future, with the usage of HSLA alloys, new alloy steels, and other medium-thick and thick plate materials, more parameters will need to be established to better meet new needs. In the aerospace and aviation sectors, hybrid

welding can help to minimize defects in aircraft plates made from materials like aluminum and titanium alloys, significantly improving the stability of aircraft fuselages. Therefore, enhancing the adaptability of hybrid welding technology to accommodate diverse materials is a future challenge. Whether addressing dissimilar steel welding or the high-temperature resistance needed for corrosion resistance and high fatigue strength, the technology must be adjusted and optimized. Currently, the rapid advancement of mechanical engineering in medium-thick and thick plate welding technology has imposed higher requirements on the field. The bevel processing of thick plates is particularly complex; improper processing can adversely affect welding stability and lead to defects. Laser–arc hybrid welding technology aligns well with industry needs. Future research should prioritize specific technological innovations, such as the real-time monitoring of the hybrid welding process and the development of high-power, low-cost laser sources. Advances in real-time monitoring and intelligent systems are essential for enhancing welding precision and efficiency, as these technologies facilitate automatic adjustments to the welding process based on various parameters and environmental conditions. Although numerical simulations have been employed to predict welding defects, the existing models may not fully correspond to real-world scenarios. Therefore, it is crucial to develop more adaptable and simplified models to enhance hybrid welding quality. A deeper understanding of these factors will unlock the full potential of hybrid welding, positioning it as the most efficient and cost-effective solution for a wide range of industrial applications in the future.

Author Contributions: Conceptualization, Y.H. and Z.Y.; methodology, Y.H.; validation, Y.H., X.S. and R.D.; formal analysis, J.X.; investigation, W.W. and L.C.; resources, W.W. and M.S.; data cu-ration, J.X.; writing—original draft preparation, X.S. and M.S.; writing—review and editing, Y.H., Z.Y., L.C. and S.C.; visualization, S.C.; supervision, R.D. and S.C.; project administration, Z.Y.; funding acquisition, Z.Y. All authors have read and agreed to the published version of the manuscript.

Funding: This study has been supported by the National Natural Science Foundation of China (Grant No. 51905231) and, the China Postdoctoral Science Foundation (Grant No. 2020M670943).

Data Availability Statement: No new data were created or analyzed in this study. Data sharing is not applicable to this article.

Conflicts of Interest: The authors declare that the research was conducted in the absence of any commercial or financial relationships that could be construed as a potential conflict of interest.

Abbreviations

LAHW, laser–arc hybrid welding; **AW**, arc welding; **LW**, laser welding; **HAZ**, heat-affected zone; **TIG**, tungsten–inert gas; **MIG**, metal–inert gas; **MAG**, metal–active gas; **PAW**, plasma arc welding; **CW**, continuous wave; **PW**, pulsed wave; **YAG**, yttrium aluminum garnet; **HLT**, laser–TIG hybrid welding; **HLM**, laser–MIG hybrid welding; **HLPW**, laser–plasma arc hybrid welding; $\mathbf{D_{LA}}$, the distance between the laser and the arc; **FEM**, finite element modeling; **FZ**, fusion zone; **BM**, base material; **STA**, solution aging treatment; **O-LAHW**, oscillating laser–arc hybrid welding; **LAHM**, laser–arc hybrid additive manufacturing; **WAAM**, wire arc additive manufacturing.

References

1. Le Guen, E.; Fabbro, R.; Carin, M.; Coste, F.; Le Masson, P. Analysis of hybrid Nd: Yag laser-MAG arc welding processes. *Opt. Laser Technol.* **2011**, *43*, 1155–1166. [CrossRef]
2. Ishide, T.; Tsubota, S.; Watanabe, M. Latest MIG, TIG, arc-YAG laser hybrid welding systems for various welding products. In Proceedings of the 1st International Symposium on High-Power Laser Macroprocessing, Osaka, Japan, 27–31 May 2002; SPIE: Bellingham, WA, USA, 2003; pp. 347–352.
3. Wang, J.; Sun, Q.; Zhang, T.; Zhang, S.; Liu, Y.; Feng, J. Arc characteristics in alternating magnetic field assisted narrow gap pulsed GTAW. *J. Mater. Process. Technol.* **2018**, *254*, 254–264. [CrossRef]

4. Paranthaman, V.; Srikanth, R.; Rajasekar, E. A systematic review of fatigue behaviour of laser welding titanium alloys. *Mater. Today Proc.* **2021**, *39*, 520–523. [CrossRef]
5. Stavridis, J.; Papacharalampopoulos, A.; Stavropoulos, P. Quality assessment in laser welding: A critical review. *Int. J. Adv. Manuf. Technol.* **2018**, *94*, 1825–1847. [CrossRef]
6. Gao, M.; Kawahito, Y.; Kajii, S. Observation and understanding in laser welding of pure titanium at subatmospheric pressure. *Opt. Express* **2017**, *25*, 13539–13548. [CrossRef]
7. Silva, R.G.N.; de Paço, C.M.M.; Rodrigues, M.B.; Sousa, R.A. A comparison between LBW and hybrid laser-GMAW processes based on microstructure and weld geometry for hardenable steels. *Int. J. Adv. Manuf. Technol.* **2020**, *110*, 2801–2814. [CrossRef]
8. Kurzynowski, T.; Gruber, K.; Stopyra, W.; Kuźnicka, B.; Chlebus, E. Correlation between process parameters, microstructure and properties of 316L stainless steel processed by selective laser melting. *Mater. Sci. Eng. A* **2018**, *718*, 64–73. [CrossRef]
9. Wang, J.Y.; Qi, T.; Zhong, C.L.; Zhang, H.; Li, X.R.; Liu, F.D. Study on seam nitrogen behavior of high nitrogen steel hybrid welding. *Optik* **2021**, *242*, 167026. [CrossRef]
10. Shu, Z.; Duan, Z.; Sun, D.; Li, Y.; Gao, D.; Li, H. Study on microstructures and mechanical properties of laser-arc hybrid welded S355J2W+N steel. *Opt. Laser Technol.* **2014**, *59*, 11–18.
11. Hong, K.; Shin, Y.C. Prospects of laser welding technology in the automotive industry: A review. *J. Mater. Process. Technol.* **2017**, *245*, 46–69. [CrossRef]
12. Gumenyuk, A.; Rethmeier, M. Developments in hybrid laser-arc welding technology. In *Handbook of Laser Welding Technologies*; Katayama, S., Ed.; Woodhead Publishing: Cambridge, UK, 2013; pp. 505–521. [CrossRef]
13. Lippold, J.C. *Welding Metallurgy and Weldability*; John Wiley & Sons: Hoboken, NJ, USA, 2014.
14. Zheng, J.; Meng, Y.; Ke, Y.; Zhou, Z.; Ge, C.; Xie, Y.; Guo, K.; Shao, C.; Lu, F.; Chen, H. Effect of beam oscillating amplitude on formation characteristics and mechanical properties of laser-arc hybrid welded 8-mm-thick aluminum alloy T-joints. *Opt. Laser Technol.* **2025**, *186*, 112676. [CrossRef]
15. Subashini, L.; Prabhakar, K.V.; Gundakaram, R.C.; Ghosh, S.; Padmanabham, G. Single pass laser arc hybrid welding of maraging steel thick sections. *Mater. Manuf. Process.* **2016**, *31*, 2186–2198. [CrossRef]
16. Wang, D.; Dong, Y.; Liu, L.; Zhu, M.; Wang, H.; Liu, C. Effect of pulsed laser and laser-arc hybrid on aluminum/steel riveting-welding hybrid bonding technology. *J. Mater. Res. Technol.* **2022**, *17*, 1043–1053. [CrossRef]
17. Berdnikova, O.; Jönsson, M.; Andren, H.; Kaplan, A.F. Laser and hybrid laser-arc welding of high-strength steel N-A-XTRA-70. *Mater. Sci. Forum.* **2016**, *870*, 630–635. [CrossRef]
18. Bunaziv, I.; Akselsen, O.M.; Ren, X.; Salminen, A. Hybrid welding possibilities of thick sections for Arctic applications. *Phys. Procedia* **2015**, *78*, 74–83. [CrossRef]
19. Zhan, X.; Li, Y.; Ou, W.; Yu, F.; Chen, J.; Wei, Y. Comparison between hybrid laser-MIG welding and MIG welding for the invar36 alloy. *Opt. Laser Technol.* **2016**, *85*, 75–84. [CrossRef]
20. Yan, S.; Nie, Y.; Zhu, Z.; Chen, H.; Gou, G.; Yu, J.; Wang, G. Characteristics of microstructure and fatigue resistance of hybrid fiber laser-MIG welded Al-Mg alloy joints. *Appl. Surf. Sci.* **2014**, *298*, 12–18. [CrossRef]
21. Acherjee, B. Hybrid laser arc welding: State-of-art review. *Opt. Laser Technol.* **2018**, *99*, 60–71. [CrossRef]
22. Steen, W.M.; Eboo, M. Arc augmented laser welding. *J. Appl. Phys.* **1979**, *50*, 2530–2531.
23. Bunaziv, I.; Akselsen, O.M.; Ren, X.; Nyhus, B.; Eriksson, M. Laser beam and laser-arc hybrid welding of aluminum alloys. *Metals* **2021**, *11*, 1150. [CrossRef]
24. Kim, Y.; Kil, S. Recent technological tendency of the laser/arc hybrid welding. *J. Weld. Join.* **2013**, *31*, 4–15. [CrossRef]
25. Liu, S.; Li, Y.; Liu, F.; Zhang, H.; Ding, H. Effects of the relative positioning of energy sources on weld integrity for hybrid laser arc welding. *Opt. Lasers Eng.* **2016**, *81*, 87–96. [CrossRef]
26. Faraji, A.H.; Moradi, M.; Goodarzi, M.; Colucci, P.; Maletta, C. An investigation on the capability of hybrid Nd: YAG laser-TIG welding technology for AA2198 Al-Li alloy. *Opt. Lasers Eng.* **2017**, *96*, 1–6. [CrossRef]
27. Huang, L.; Wu, D.; Hua, X.; Liu, S.; Jiang, Z.; Li, F.; Wang, H.; Shi, S. Effect of the welding direction on the microstructural characterization in fiber laser-GMAW hybrid welding of 5083 aluminum alloy. *J. Manuf. Process.* **2018**, *31*, 514–522. [CrossRef]
28. Bunaziv, I.; Akselsen, O.M.; Salminen, A.; Unt, A. The fiber laser-MIG hybrid welding of 5 mm 5083 aluminum alloy. *J. Mater. Process. Technol.* **2016**, *233*, 107–114. [CrossRef]
29. Liu, L.; Hao, X.; Song, G. A new laser-arc hybrid welding technique based on energy conservation. *Mater. Trans.* **2006**, *47*, 1611–1614. [CrossRef]
30. Zhao, Y.; Zhan, X.; Zhou, X.; Liu, T.; Kang, Y. Effect of heat input on macro morphology and porosity of laser-MIG hybrid welded joint for 5A06 aluminum alloy. *Int. J. Adv. Manuf. Technol.* **2021**, *115*, 4035–4045. [CrossRef]
31. Kapil, A.; Suga, T.; Tanaka, M.; Sharma, A. Towards hybrid laser-arc based directed energy deposition: Understanding bead formation through mathematical modeling for additive manufacturing. *J. Manuf. Process.* **2022**, *76*, 457–474. [CrossRef]
32. Atabaki, M.M.; Nikodinovski, M.; Chenier, P.; Ma, J.; Liu, W.; Kovacevic, R. Experimental and numerical investigations of hybrid laser arc welding of aluminum alloys in the thick T-joint configuration. *Opt. Lasers Eng.* **2014**, *59*, 68–92. [CrossRef]

33. Liu, F.; Yang, B.; Sun, H.; Wang, H.; Tan, C.; Wang, G.; Chen, B. Mechanism investigation for the influence of laser power on droplet transfer behaviors in laser-MIG hybrid welding. *Opt. Laser Technol.* **2023**, *157*, 108750. [CrossRef]
34. Fan, H.; Zhou, P.; Li, J.; Huang, J.; Ni, Y.; Hui, Y. Microstructure and mechanical properties of arc-zone and laser zone of TC4 titanium alloy laser–TIG hybrid welded joint. *Metals* **2022**, *12*, 1854. [CrossRef]
35. Li, R.; Zhang, F.; Sun, T.; Liu, B.; Chen, S.; Tian, Y. Investigation of strengthening mechanism of commercially pure titanium joints fabricated by autogenously laser beam welding and laser-MIG hybrid welding processes. *Int. J. Adv. Manuf. Technol.* **2019**, *101*, 377–389. [CrossRef]
36. Möller, F.; Thomy, C. Interaction effects between laser beam and plasma arc in hybrid welding of aluminum. *Phys. Procedia* **2013**, *41*, 81–89. [CrossRef]
37. Zhang, C.; Gao, M.; Jiang, M.; Zeng, X. Effect of weld characteristic on mechanical strength of laser-arc hybrid-welded Al-Mg-Si-Mn aluminum alloy. *Metall. Mater. Trans. A* **2016**, *47*, 5438–5449. [CrossRef]
38. Umroh, B.; Ginting, A.; Rahman, M.N.A. CO_2 laser machining on alumina ceramic: A review. *IOP Conf. Ser. Mater. Sci. Eng.* **2020**, *1003*, 012131. [CrossRef]
39. Vemanaboina, H.; Babu, M.M.; Prerana, I.C.; Gundabattini, E.; Yelamasetti, B.; Saxena, K.K.; Salem, K.H.; Khan, M.I.; Eldin, S.M.; Agrawal, M.K. Evaluation of residual stresses in CO_2 laser beam welding of SS316L weldments using FEA. *Mater. Res. Express* **2023**, *10*, 016509. [CrossRef]
40. Prabakaran, M.P.; Kannan, G.R.; Pandiyarajan, R. Effects of Welding Speed on Microstructure and Mechanical Properties of CO_2 Laser Welded Dissimilar Butt Joints between Low Carbon Steel and Austenitic Stainless Steel. *Adv. Mater. Process. Technol.* **2020**, *8* (Suppl. S1), 1–12. [CrossRef]
41. Zhu, Z.; Lv, S.; Zhang, H.; Hui, Y.; Lei, H.; Li, Q. Highly efficient actively Q-switched Nd: YAG laser. *Opt. Express* **2021**, *29*, 32325–32332. [CrossRef]
42. Li, H.N.; Xie, K.G.; Wu, B.; Zhu, W.Q. Generation of textured diamond abrasive tools by continuous-wave CO_2 laser: Laser parameter effects and optimization. *J. Mater. Process Technol.* **2020**, *275*, 116279. [CrossRef]
43. Sharma, A.; Yadava, V. Experimental analysis of Nd: YAG laser cutting of sheet materials—A review. Opt. *Laser Technol.* **2018**, *98*, 264–280. [CrossRef]
44. Pavan, A.R.; Arivazhagan, B.; Vasudevan, M.; Prasanthi, T.N.; Sudha, C. Study on the microstructure and mechanical properties of hybrid laser + MIG welded joints of 316LN stainless steel. *Opt. Laser Technol.* **2023**, *163*, 109410. [CrossRef]
45. Xie, J.; Cai, C.; Liang, Y.; Liu, Z.; Ma, Y. Microstructure and mechanical properties of heat affected zone of laser-MAG hybrid welded low carbon bainitic steel joints. *Opt. Laser Technol.* **2022**, *148*, 107729. [CrossRef]
46. Wang, H.; Liu, X.; Liu, L. Research on Laser-TIG Hybrid Welding of 6061-T6 aluminum alloys joint and post heat treatment. *Metals* **2020**, *10*, 130. [CrossRef]
47. Cai, D.; Liu, W.; Luo, Z.; Gao, S.; Chen, C.; Zhang, Y. Inhibition of undercut defect and its effect on tensile fracture mechanism of coaxial laser-plasma hybrid welding without filler. *Opt. Laser Technol.* **2024**, *175*, 110770. [CrossRef]
48. Lahdo, R.; Nothdurft, S.; Hermsdorf, J.; Urbanek, P.; Puschmann, M.; Riedel, F.; Overmeyer, L.; Kaierle, S. Investigations on microstructure and mechanical properties of laser beam-submerged arc hybrid welded butt joints of duplex stainless steel S31083 (t = 16 mm) depending on the energy per unit length. *Procedia CIRP* **2022**, *111*, 409–414. [CrossRef]
49. Gomes, A.S.L.; Moura, A.L.; de Araújo, C.B.; Raposo, E.P. Recent advances and applications of random lasers and random fiber lasers. *Prog. Quantum Electron.* **2021**, *78*, 100343. [CrossRef]
50. Dragic, P.D.; Cavillon, M.; Ballato, J.J.A. Materials for optical fiber lasers: A review. *Appl. Phys. Rev.* **2018**, *5*, 041303. [CrossRef]
51. Liu, Z.; Ma, P.; Su, R.; Tao, R.; Ma, Y.; Wang, X.; Zhou, P. High-Power Coherent Beam Polarization Combination of Fiber Lasers: Progress and Prospect [Invited]. *J. Opt. Soc. Am. B* **2017**, *34*, A7–A14. [CrossRef]
52. Nemova, G. Brief review of recent developments in fiber lasers. *Appl. Sci.* **2024**, *14*, 2323. [CrossRef]
53. García de Arquer, F.P.; Talapin, D.V.; Klimov, V.I.; Arakawa, Y.; Bayer, M.; Sargent, E.H. Semiconductor quantum dots: Technological progress and future challenges. *Science* **2021**, *373*, 1147–1153. [CrossRef]
54. Zhang, Q.; Shang, Q.; Su, R.; Do, T.T.H.; Xiong, Q. Halide perovskite semiconductor lasers: Materials, cavity design, and low threshold. *Nano Lett.* **2021**, *21*, 1903–1914. [CrossRef] [PubMed]
55. Ning, J.; Zhang, L.J.; Na, S.J.; Yin, X.Q.; Niu, J.; Zhang, J.X.; Wang, H.R. Numerical study of the effect of laser-arc distance on laser energy coupling in pulsed Nd: YAG laser/TIG hybrid welding. *Int. J. Adv. Manuf. Technol.* **2017**, *91*, 1129–1143. [CrossRef]
56. Verma, R.P.; Pandey, K.N.; András, K.; Khargotra, R.; Singh, T. Difficulties and redressal in joining of aluminum alloys by GMA and GTA welding: A review. *J. Mater. Res. Technol.* **2023**, *23*, 2576–2586. [CrossRef]
57. Sahoo, A.; Tripathy, S. Development in plasma arc welding process: A review. *Mater. Today Proc.* **2021**, *41*, 363–368. [CrossRef]
58. Echezona, N.; Akinlabi, S.A.; Jen, T.C.; Fatoba, O.S.; Hassan, S.; Akinlabi, E.T. TIG welding of dissimilar steel: A review. In *Advances in Material Science and Engineering, Lecture Notes in Mechanical Engineering*; Awang, M., Emamian, S.S., Eds.; Springer: Singapore, 2021. [CrossRef]

59. Ardika, R.D.; Triyono, T.; Muhayat, N. A review of porosity in aluminum welding. *Procedia Struct. Integr.* **2021**, *33*, 171–180. [CrossRef]
60. Wu, H.; Chang, Y.; Mei, Q.; Liu, D. Research advances in high-energy TIG arc welding. *Int. J. Adv. Manuf. Technol.* **2019**, *33*, 391–410. [CrossRef]
61. Olivares, E.A.G.; Silva, R.H.G.; Dutra, J.C. Study of keyhole TIG welding by comparative analysis of two high-productivity torches for joining medium-thickness carbon steel plates. *Weld. Int.* **2017**, *31*, 337–347. [CrossRef]
62. Vemanaboina, H.; Gundabattini, E.; Akella, S.; Rao, A.U.; Buddu, R.K.; Ferro, P.; Berto, F. Mechanical and metallurgical properties of CO_2 laser beam INCONEL 625 welded joints. *Appl. Sci.* **2021**, *11*, 7002. [CrossRef]
63. Anbarasu, P.; Yokeswaran, R.; Godwin Antony, A.; Sivachandran, S. Investigation of filler material influence on hardness of TIG welded joints. *Mater. Today Proc.* **2020**, *21*, 964–967. [CrossRef]
64. Casalino, G.; Dassisti, M.; Perulli, P. FEM model for TIG hybrid laser butt welding of 6 mm thick austenitic to martensitic stainless steels. *Procedia CIRP* **2020**, *88*, 116–121. [CrossRef]
65. Yan, J.; Gao, M.; Zeng, X. Study on microstructure and mechanical properties of 304 stainless steel joints by TIG, laser, and laser-TIG hybrid welding. *Opt. Lasers Eng.* **2010**, *48*, 512–517. [CrossRef]
66. Silva, R.G.N.; Pereira, M.; Rodrigues, M.B.; Pereira, A.D.; Schwedersky, M.B. Electric evaluation of hybrid laser-TIG welding: Interaction between arc and laser plume. *J. Laser Appl.* **2020**, *32*, 022012. [CrossRef]
67. Avilov, V.; Decker, I.; Pursch, H.; Wendelstorf, J. Study of a laser-enhanced welding arc using advanced split anode technique. *Weld. J.* **1994**, *11*, 112–123.
68. Dutra, J.C.; Gonçalves e Silva, R.H.; Riffel, K.C.; Marques, C. High-performance GMAW process for deep penetration applications. *Weld. World* **2020**, *64*, 999–1009. [CrossRef]
69. Ribeiro, R.A.; Assunção, P.D.C.; Dos Santos, E.B.F.; Braga, E.M.; Gerlich, A.P. An overview on the cold wire pulsed gas metal arc welding. *Weld. World* **2020**, *64*, 123–140. [CrossRef]
70. Yang, Z.; Chen, Y.; Zhang, Z.; Fang, C.; Xu, K.; He, P.; Zhang, Z. Research on the Sidewall Penetration Mechanisms of Cable-Type Welding Wire Narrow Gap GMAW Process. *Int. J. Adv. Manuf. Technol.* **2022**, *120*, 2443–2455. [CrossRef]
71. Bidi, L.; Le Masson, P.; Cicala, E.; Primault, C. Experimental design method to the weld bead geometry optimization for hybrid laser-MAG welding in a narrow chamfer configuration. *Opt. Lasers Technol.* **2017**, *89*, 114–125. [CrossRef]
72. Pan, Q.; Mizutani, M.; Kawahito, Y.; Katayama, S. Effect of shielding gas on laser-MAG arc hybrid welding results of thick high-tensile-strength steel plates. *Weld. World* **2016**, *60*, 653–664. [CrossRef]
73. Cai, C.; Yu, J.; Chen, Z.; Li, Z.; Chen, H.; Tang, P.; Xiong, F. Welding Process Stability in Narrow-Gap Oscillating Laser-MIG Hybrid Welding of Titanium Alloys with Various Oscillating Patterns. *J. Manuf. Process.* **2025**, *133*, 151–162. [CrossRef]
74. Subashini, L.; Prabhakar, K.V.P.; Ghosh, S.; Padmanabham, G. Comparison of laser-MIG hybrid and autogenous laser welding of M250 maraging steel thick sections—Understanding the role of filler wire addition. *Int. J. Adv. Manuf. Technol.* **2020**, *107*, 1581–1594. [CrossRef]
75. Jiang, Z.; Hua, X.; Huang, L.; Wu, D.; Li, F.; Zhang, Y. Double-sided hybrid laser-MIG welding plus MIG welding of 30-mm-thick aluminum alloy. *Int. J. Adv. Manuf. Technol.* **2018**, *97*, 903–913. [CrossRef]
76. Huang, H.; Zhang, P.; Yan, H.; Liu, Z.; Yu, Z.; Wu, D.; Shi, H.; Tian, Y. Research on weld formation mechanism of laser-MIG arc hybrid welding with butt gap. *Opt. Lasers Technol.* **2021**, *133*, 106530. [CrossRef]
77. Oyyaravelu, R.; Kuppan, P.; Arivazhagan, N. Comparative study on metallurgical and mechanical properties of laser and laser-arc-hybrid welding of HSLA steel. *Mater. Today Proc.* **2018**, *5*, 12693–12705. [CrossRef]
78. Tashiro, S. Interaction Mechanism of Arc, Keyhole, and Weld Pool in Keyhole Plasma Arc Welding: A Review. *Materials* **2024**, *17*, 1348. [CrossRef]
79. Ribeiro, R.A.; Dos Santos, E.B.F.; Assunção, P.D.C.; Braga, E.M.; Gerlich, A.P. Cold wire gas metal arc welding: Droplet transfer and geometry. *Weld. J.* **2019**, *98*, 135s–149s. [CrossRef]
80. Jiang, F.; Li, C.; Chen, S.J. Experimental investigation on heat transfer of different phases in variable polarity plasma arc welding. *Weld. World* **2019**, *63*, 1153–1162. [CrossRef]
81. Khanna, P.; Singh, S.J.; Kumar, D.; Suman, S. Investigation of Bead Geometry Parameters During MIG Welding of Stainless Steel 202 Plates. In *Recent Developments in Mechanics and Design*; INCOME 2023; Lecture Notes in Mechanical Engineering; Singh, D.K., Hegde, S., Mishra, A., Eds.; Springer: Singapore, 2024. [CrossRef]
82. Wu, D.; Tashiro, S.; Hua, X.; Tanaka, M. Analysis of the energy propagation in the keyhole plasma arc welding using a novel fully coupled plasma arc-keyhole-weld pool model. *Int. J. Heat Mass Transf.* **2019**, *141*, 604–614. [CrossRef]
83. Korzhyk, V.; Bushma, O.; Khaskin, V.; Dong, C.; Sydorets, V. Analysis of the current state of the processes of hybrid laser-plasma welding. In *Proceedings of the Second International Conference on Mechanics, Materials and Structural Engineering (ICMMSE 2017), Beijing, China, 14–16 April 2017*; Atlantis Press: Dordrecht, The Netherlands, 2017; pp. 80–90. [CrossRef]
84. Meng, Y.; Gao, M.; Zeng, X.Y. Effects of arc types on the laser-arc synergic effects of hybrid welding. *Opt. Express* **2018**, *26*, 14775–14785. [CrossRef]

85. Zou, J.L.; Wu, S.K.; Xiao, R.S.; Li, F. Effects of a paraxial TIG arc on high-power fiber laser welding. *Mater. Des.* **2015**, *86*, 321–327. [CrossRef]
86. Zhang, C.; Gao, M.; Zeng, X.Y. Influences of synergy effect between laser and arc on laser-arc hybrid welding of aluminum alloys. *Opt. Laser Technol.* **2019**, *120*, 105766. [CrossRef]
87. Liu, W.; Ma, J.; Yang, G.; Kovacevic, R. Hybrid laser-arc welding of advanced high-strength steel. *J. Mater. Process. Technol.* **2014**, *214*, 2823–2833. [CrossRef]
88. Gao, M.; Zeng, X.Y.; Hu, Q.W. Effects of welding parameters on melting energy of CO_2 laser–GMA hybrid welding. *Sci. Technol. Weld. Join.* **2006**, *11*, 517–522. [CrossRef]
89. Meng, Y.; Gao, M.; Zeng, X.Y. Quantitative analysis of synergic effects during laser-arc hybrid welding of AZ31 magnesium alloy. *Opt. Laser Eng.* **2018**, *111*, 183–192. [CrossRef]
90. Gao, M.; Zeng, X.; Hu, Q. Effects of gas shielding parameters on weld penetration of CO_2 laser-TIG hybrid welding. *J. Mater. Process. Technol.* **2007**, *184*, 177–183. [CrossRef]
91. Gao, Z.M.; Jiang, P.; Wang, C.; Shao, X.; Pang, S.; Zhou, Q.; Li, X.; Wang, Y. Study on droplet transfer and weld quality in laser-MIG hybrid welding of 316L stainless steel. *Int. J. Adv. Manuf. Technol.* **2017**, *88*, 483–493. [CrossRef]
92. Zhang, S.W.; Wang, Y.; Zhu, M.; Feng, Y.; Nie, P.; Li, Z. Effects of heat source arrangements on Laser-MAG hybrid welding characteristics and defect formation mechanism of 10CrNi3MoV steel. *J. Manuf. Process.* **2020**, *58*, 563–573. [CrossRef]
93. Moradi, M.; Ghoreishi, M.; Frostevarg, J.; Kaplan, A.F. An investigation on stability of laser hybrid arc welding. *Opt. Laser Eng.* **2013**, *51*, 481–487. [CrossRef]
94. Kouraytem, N.; Li, X.; Cunningham, R.; Zhao, C.; Parab, N.; Sun, T.; Rollett, A.D.; Spear, A.D.; Tan, W. Effect of laser-matter interaction on molten pool flow and keyhole dynamics. *Phys. Rev. Appl.* **2019**, *11*, 064054. [CrossRef]
95. Shrestha, S.; Chou, K.Y. A numerical study on the keyhole formation during laser powder bed fusion process. *J. Manuf. Sci. Eng.* **2019**, *141*, 101002. [CrossRef]
96. Ning, J.; Zhang, L.J.; Zhang, L.L.; Long, J.; Yin, X.Q.; Zhang, J.X.; Na, S.J. Effects of power modulation on behaviors of molten pool and keyhole during laser–arc hybrid welding of pure copper. *Mater. Des.* **2020**, *194*, 108829. [CrossRef]
97. Wu, C.S.; Zhang, H.T.; Chen, J. Numerical simulation of keyhole behaviors and fluid dynamics in laser–gas metal arc hybrid welding of ferrite stainless steel plates. *J. Manuf. Process.* **2017**, *25*, 235–245. [CrossRef]
98. Courtois, M.; Carin, M.; Le Masson, P.; Gaied, S.; Balabane, M. A complete model of keyhole and melt pool dynamics to analyze instabilities and collapse during laser welding. *J. Laser Appl.* **2014**, *26*, 042001. [CrossRef]
99. Tan, C.W.; Dong, Y.; Sun, H.F.; Liu, F.; Han, X.; Dong, Q.; Chen, B.; Song, X. Numerical study on weld pool behaviors and keyhole dynamics in magnetic-field-assisted laser-arc hybrid welding of aluminum alloy. *J. Mater. Res. Technol.* **2023**, *26*, 6446–6461. [CrossRef]
100. Xu, X.K.; Song, G.; Zhao, S.; Liu, L.M. Effect of distance between the heat sources on energy transfer behavior in keyhole during laser-GTA welding titanium alloy. *J. Manuf. Process.* **2020**, *55*, 317–325. [CrossRef]
101. Xu, G.X.; Li, P.F.; Cao, Q.N.; Hu, Q.; Gu, X.; Du, B. Modelling of fluid flow phenomenon in laser + GMAW hybrid welding of aluminum alloy considering three phase coupling and arc plasma shear stress. *Opt. Laser Technol.* **2018**, *100*, 244–255. [CrossRef]
102. Miyagi, M.; Wang, J. Keyhole dynamics and morphology visualized by in-situ X-ray imaging in laser melting of austenitic stainless steel. *J. Mater. Process. Technol.* **2020**, *282*, 116673. [CrossRef]
103. Kaplan, A.F.H. Local flashing events at the keyhole front in laser welding. *Opt. Laser Eng.* **2015**, *68*, 35–41. [CrossRef]
104. Zhang, L.J.; Zhang, J.X.; Gumenyuk, A.; Rethmeier, M.; Na, S.J. Numerical simulation of full penetration laser welding of thick steel plate with high power high brightness laser. *J. Mater. Process. Technol.* **2014**, *214*, 1710–1720. [CrossRef]
105. Rong, Y.M.; Xu, J.J.; Cao, H.Y.; Zheng, H.; Huang, Y.; Zhang, G. Influence of steady magnetic field on dynamic behavior mechanism in full penetration laser beam welding. *J. Manuf. Process.* **2017**, *26*, 399–406. [CrossRef]
106. Li, M.; Xu, J.; Huang, Y.; Rong, Y. Improving keyhole stability by external magnetic field in full penetration laser welding. *JOM* **2018**, *70*, 1261–1266. [CrossRef]
107. Zhan, X.H.; Liu, X.; Li, Y.; Zhao, Y.; Wang, J. Molten pool behavior and solidification characterization in steady magnetic field assisted laser-MIG hybrid welding of aluminum alloy. *J. Manuf. Process.* **2022**, *84*, 622–638. [CrossRef]
108. Liu, F.Y.; Xu, B.X.; Song, K.; Tan, C.; Zhao, H.; Wang, G.; Chen, B.; Song, X. Improvement of penetration ability of heat source for 316 stainless steel welds produced by alternating magnetic field assisted laser-MIG hybrid welding. *J. Mater. Process. Technol.* **2022**, *299*, 117329. [CrossRef]
109. Huang, L.J.; Hua, X.; Wu, D.; Li, F. Numerical study of keyhole instability and porosity formation mechanism in laser welding of aluminum alloy and steel. *J. Mater. Process. Technol.* **2018**, *252*, 421–431. [CrossRef]
110. Wang, X.; Huang, Y.; Zhang, Y. Droplet transfer model for laser-enhanced GMAW. *Int. J. Adv. Manuf. Technol.* **2013**, *64*, 207–217. [CrossRef]
111. Liu, Q.Y.; Wu, D.; Wang, Q.; Zhang, P.; Yan, H.; Sun, T.; Zeng, J.; Yan, M.; Liu, Z.; Li, R. Research status of stability in dynamic process of laser-arc hybrid welding based on droplet transfer behavior: A review. *Coatings* **2023**, *13*, 205. [CrossRef]

112. Liu, S.Y.; Liu, F.D.; Xu, C.Y.; Zhang, H. Experimental investigation on arc characteristic and droplet transfer in CO_2 laser–metal arc gas (MAG) hybrid welding. *Int. J. Heat Mass Transf.* **2013**, *62*, 604–611. [CrossRef]
113. Li, R.; Yue, J.; Sun, R.; Mi, G.; Wang, C.; Shao, X. A study of droplet transfer behavior in ultra-narrow gap laser arc hybrid welding. *Int. J. Adv. Manuf. Technol.* **2016**, *87*, 2997–3008. [CrossRef]
114. Zhang, W.; Hua, X.; Liao, W.; Li, F.; Wang, M. Behavior of the plasma characteristic and droplet transfer in CO_2 laser–GMAW-P hybrid welding. *Int. J. Adv. Manuf. Technol.* **2014**, *72*, 935–942. [CrossRef]
115. Cai, C.; Feng, J.C.; Li, L.Q.; Chen, Y. Influence of laser on the droplet behavior in short-circuiting, globular, and spray modes of hybrid fiber laser-MIG welding. *Opt. Laser Technol.* **2016**, *83*, 108–118. [CrossRef]
116. Liu, S.Y.; Zhang, F.; Dong, S.; Zhang, H.; Liu, F. Characteristics analysis of droplet transfer in laser-MAG hybrid welding process. *Int. J. Heat Mass Transf.* **2018**, *121*, 805–811. [CrossRef]
117. Gao, X.D.; Wang, Y.; Chen, Z.Q.; Ma, B.; Zhang, Y. Analysis of welding process stability and weld quality by droplet transfer and explosion in MAG-laser hybrid welding process. *J. Manuf. Process.* **2018**, *32*, 522–529. [CrossRef]
118. Chen, Y.B.; Feng, J.C.; Li, L.Q.; Li, Y.; Chang, S. Effects of welding positions on droplet transfer in CO_2 laser–MAG hybrid welding. *Int. J. Adv. Manuf. Technol.* **2013**, *68*, 1351–1359. [CrossRef]
119. Jing, H.; Ye, X.; Hou, X.; Qian, X.; Zhang, P.; Yu, Z.; Wu, D.; Fu, K. Influence of Laser Power and Butt Gap on Droplet Transfer and Weld Formation in Laser-Arc Hybrid Welding. *J. Phys. Conf. Ser.* **2021**, *2002*, 012009. [CrossRef]
120. Chen, Y.; Yang, Z.; Ni, Z.; Xu, J.M.; Dong, S.W.; Xu, G.X.; Chen, S.J. Effect of distance between heat sources on droplet transfer behavior and weld formation of AH36 during laser and CWW GMAW arc hybrid welding. *J. Iron Steel Res. Int.* **2024**, *31*, 3069–3079. [CrossRef]
121. Cai, B.; Fu, J.; Zhao, Y.; Chen, F.; Qin, Y.; Song, S. Effect of alternating magnetic field on arc plasma characteristics and droplet transfer during narrow gap laser-MIG hybrid welding. *Metals* **2021**, *11*, 1712. [CrossRef]
122. Liu, Q.; Wu, D.; Wang, Q.; Zhang, P.; Yan, H.; Sun, T.; Yan, M.; Zeng, J.; Liu, Z.; Feng, J.; et al. Influencing mechanism of high speed on the droplet transfer and process stability during high-power laser-arc hybrid welding. *Int. J. Adv. Manuf. Technol.* **2023**, *128*, 4427–4442. [CrossRef]
123. Zhu, Z.W.; Ma, X.Q.; Wang, C.M.; Mi, G. Modification of droplet morphology and arc oscillation by magnetic field in laser-MIG hybrid welding. *Opt. Laser Eng.* **2020**, *131*, 106138. [CrossRef]
124. Gui, X.; Gao, X.; Zhang, Y.; Wu, J. Investigation of welding parameters effects on temperature field and structure field during laser-arc hybrid welding. *Mod. Phys. Lett. B* **2022**, *36*, 2150467. [CrossRef]
125. Zhang, C.; Zhang, H.; Wang, L.; Gao, M.; Zeng, X. Microcracking and mechanical properties in laser-arc hybrid welding of wrought Al-6Cu aluminum alloy. *Metall. Mater. Trans. A* **2018**, *49*, 4441–4445. [CrossRef]
126. Lv, X.Z.; Liu, L.M. Microstructure and mechanical performance of AZ31/6061 lap joints welded by laser-TIG hybrid welding with Zn-Al alloy filler metal. *J. Magnes. Alloy* **2023**, *12*, 3325–3338. [CrossRef]
127. Zhang, W.; Hua, X.; Liao, W.; Li, F.; Wang, M. Study of metal transfer in CO_2 laser + GMAW-P hybrid welding using argon–helium mixtures. *Opt. Laser Technol.* **2014**, *56*, 158–166. [CrossRef]
128. Turichin, G.; Kuznetsov, M.; Klimova-Korsmik, O.; Sklyar, M.; Zhitenev, A.; Kurakin, A.; Pozdnyakov, A. Laser-Arc hybrid welding perspective ultra-high strength steels: Influence of the chemical composition of weld metal on microstructure and mechanical properties. *Procedia CIRP* **2018**, *74*, 752–756. [CrossRef]
129. Gao, Y.K.; Hao, K.D.; Xu, L.Y.; Han, Y.; Zhao, L.; Ren, W.; Jing, H. Microstructure homogeneity and mechanical properties of laser-arc hybrid welded AZ31B magnesium alloy. *J. Magnes. Alloys* **2022**, *12*, 1986–1995. [CrossRef]
130. Sun, G.F.; Wang, Z.D.; Lu, Y.; Zhou, R.; Ni, Z.H.; Gu, X.; Wang, Z.G. Numerical and experimental investigation of thermal field and residual stress in laser-MIG hybrid welded NV E690 steel plates. *J. Manuf. Process.* **2018**, *34*, 106–120. [CrossRef]
131. Ragavendran, M.; Vasudevan, M. Effect of Laser and Hybrid Laser Welding Processes on the Residual Stresses and Distortion in AISI Type 316L(N) Stainless Steel Weld Joints. *Metall. Mater. Trans. B* **2021**, *52*, 2582–2603. [CrossRef]
132. Hong, X.L.; Huang, B.S.; Li, T.L.; Chen, P.; Zheng, J.N.; Zhu, Y.Y. Effects of welding speed and welding current on the residual stress and deformation of SAF 2507/316L dissimilar plasma arc welding. *J. Mater. Eng. Perform.* **2024**, *33*, 13745–13763. [CrossRef]
133. Chen, L.; Mi, G.Y.; Zhang, X.; Wang, C.M. Numerical and experimental investigation on microstructure and residual stress of multi-pass hybrid laser-arc welded 316L steel. *Mater. Des.* **2019**, *168*, 107653. [CrossRef]
134. Yang, J.; Dong, H.; Wu, G.; Xiong, F. Experimental and numerical simulation study on microstructure, residual stress, and mechanical properties of Fe–Mn–C–Cr cryogenic high-manganese steel arc-welded joint. *J. Mater. Res. Technol.* **2025**, *35*, 1335–1347. [CrossRef]
135. Hammad, A.; Churiaque, C.; Sánchez-Amaya, J.M.; Abdel-Nasser, Y. Experimental and numerical investigation of hybrid laser arc welding process and the influence of welding sequence on the manufacture of stiffened flat panels. *J. Manuf. Process.* **2021**, *61*, 527–538. [CrossRef]
136. Katayama, S. *Handbook of Laser Welding Technologies*; Woodhead Publishing: Cambridge, UK, 2013.

137. Han, R.H.; Li, Y.Y.; Lu, S.P. Macro-micro modeling and simulation for the morphological evolution of the solidification structures in the entire weld. *Int. J. Heat Mass Transf.* **2017**, *106*, 1345–1355. [CrossRef]
138. Djeloud, H.; Moussaoui, M.; Kouider, R.; Al-Kassir, A.; Carrasco-Amador, J.P. Study of the heat exchange and relaxation conditions of residual stresses due to welding of austenitic stainless steel. *Energies* **2023**, *16*, 3176. [CrossRef]
139. Schempp, P.; Rethmeier, M. Understanding grain refinement in aluminum welding. *Weld. World* **2015**, *59*, 767–784. [CrossRef]
140. Wang, L.; Gao, M.; Hao, Z. A pathway to mitigate macrosegregation of laser-arc hybrid Al-Si welds through beam oscillation. *Int. J. Heat Mass Transf.* **2020**, *151*, 119467. [CrossRef]
141. Du, Z.L.; Sun, X.C.; Ng, F.L.; Chew, Y.X.; Tan, C.L.; Bi, G.J. Thermo-metallurgical simulation and performance evaluation of hybrid laser arc welding of chromium-molybdenum steel. *Mater. Des.* **2021**, *210*, 110029. [CrossRef]
142. Chen, J.; Zhang, Z.; Liu, Y.; Zhao, X.; Chen, J.; Chen, H. Effect of the cooling rate of thermal simulation on the microstructure and mechanical properties of low-carbon bainite steel by laser-arc hybrid welding. *Coatings* **2022**, *12*, 1045. [CrossRef]
143. Munro, C.; Nolting, A.E.; Cao, X.J.; Wanjara, P. Hybrid laser-arc welding of HSLA-65 steel plate: Microstructural and mechanical property evaluation of butt welds. *Mater. Sci. Forum* **2012**, *706–709*, 2992–2997. [CrossRef]
144. Zhang, C.; Li, G.; Gao, M.; Zeng, X. Microstructure and mechanical properties of narrow gap laser-arc hybrid welded 40 mm thick mild steel. *Materials* **2017**, *10*, 106. [CrossRef]
145. Xie, L.; Shi, W.; Wu, T.; Gong, M.; Cai, D.; Han, S.; He, K. Effect of hybrid laser arc welding on the microstructure and mechanical and fracture properties of 316L sheet welded joints. *Metals* **2022**, *12*, 2181. [CrossRef]
146. Shen, L.; Chen, Y.; Zhu, H.; Lei, Y.; Qiu, C. Ti6Al4V alloy remelting by modulation laser: Deep penetration, high compactness, and metallurgical bonding with matrix. *Micromachines* **2022**, *13*, 1107. [CrossRef]
147. Chen, G.; Hirohata, M.; Hyoma, K.; Matsumoto, N.; Inose, K. Deformation and residual stress of T-shaped joints fabricated by laser-arc hybrid welding for steel bridge members. *Weld. World* **2024**, *68*, 459–473. [CrossRef]
148. Zhang, C.; Gao, M.; Zeng, X. Effect of microstructural characteristics on high cycle fatigue properties of laser-arc hybrid welded AA6082 aluminum alloy. *J. Mater. Process Technol.* **2016**, *231*, 479–487. [CrossRef]
149. Wang, Q.; Chen, H.; Qiu, P.; Zhu, Z. Residual stress and fatigue strength of hybrid laser-MIG-welded A7N01P-T4. *Metall. Mater. Trans. B* **2017**, *48*, 591–601. [CrossRef]
150. Yang, Z.; Huan, J.; Xu, K.; He, P. Effect of Polarities and Shielding Gases in CWW GMAW. *Mater. Manuf. Process.* **2024**, *39*, 227–236. [CrossRef]
151. Sathiya, P.; Mishra, M.K.; Soundararajan, R.; Shanmugarajan, B. Shielding gas effect on weld characteristics in arc-augmented laser welding process of super austenitic stainless steel. *Opt. Laser Technol.* **2013**, *45*, 46–55. [CrossRef]
152. Rao, Z.H.; Liao, S.M.; Tsai, H.L. Effects of shielding gas compositions on arc plasma and metal transfer in gas metal arc welding. *J. Appl. Phys.* **2010**, *107*, 043305. [CrossRef]
153. Zhu, Y.; Cai, Y.; Wang, M. Effects of He content in shielding gases on high-efficient hybrid laser arc welding with C-276 filler metal. *J. Mater. Process Technol.* **2022**, *299*, 117367. [CrossRef]
154. Tani, G.; Campana, G.; Fortunato, A.; Ascari, A. The influence of shielding gas in hybrid laser-MIG welding. *Appl. Surf. Sci.* **2007**, *253*, 19–25. [CrossRef]
155. Ahn, J.; He, E.; Chen, L.; Dear, J.; Davies, C. The effect of Ar and He shielding gas on fibre laser weld shape and microstructure in AA 2024-T3. *J. Manuf. Process.* **2023**, *29*, 62–73. [CrossRef]
156. Wallerstein, D.; Vaamonde, E.; Prada, A.; Torres, E.A.; Urtiga Filho, S.L.; Santos, T.F. Influence of welding gases and filler metals on hybrid laser-GMAW and Laser-FCAW welds. *Proc. Inst. Mech. Eng. C J. Mech. Eng. Sci.* **2021**, *235*, 2754–2767. [CrossRef]
157. Fang, N.; Huang, R.; Wang, X.; Tian, J.; Li, S.; Wu, P.; Xu, K.; He, P.; Wen, G.; Jiang, L. Effect of shielding gas on the microstructure and properties of laser-MAG hybrid welded joint for nickel-saving stainless steel. *Adv. Mater. Sci. Eng.* **2022**, *2022*, 9330521. [CrossRef]
158. Bai, D.; Liu, F.; Zhang, H. Effect of Welding Shielding Gas Composition on the Properties of Laser-Arc Hybrid Welding Joint of High Nitrogen Stainless Steel. *J. Phys. Conf. Ser.* **2021**, *1838*, 012020. [CrossRef]
159. Yang, X.; Chen, H.; Zhu, Z.; Cai, C.; Zhang, C. Effect of shielding gas flow on welding process of laser-arc hybrid welding and MIG welding. *J. Manuf. Process.* **2019**, *38*, 530–542. [CrossRef]
160. Chen, Y.; Yang, Z.; Xu, K.; He, P.; Shi, M.; Chen, S.; Fang, C. Effect of energy parameters on droplet transfer behavior and weld formation in laser-arc hybrid welding with cable-type welding wire. *J. Mater. Res. Technol.* **2023**, *26*, 4191–4205. [CrossRef]
161. Gao, Z.; Shao, X.; Jiang, P.; Cao, L.; Zhou, Q.; Yue, C.; Liu, Y.; Wang, C. Parameters optimization of hybrid fiber laser-arc butt welding on 316L stainless steel using Kriging model and GA. *Opt. Laser Technol.* **2016**, *83*, 153–162. [CrossRef]
162. Wang, L.; Gao, M.; Zeng, X. Experiment and prediction of weld morphology for laser oscillating welding of AA6061 aluminum alloy. *Sci. Technol. Weld. Join.* **2019**, *24*, 334–341. [CrossRef]
163. Wu, Y.; Li, Z.; Wang, X.; Feng, Y.; Wang, M.; Shan, J. Narrow groove laser-arc hybrid welding of thick-sectioned HSLA steel using laser beam oscillation. *Weld. J.* **2022**, *101*, 181–196. [CrossRef]

164. Shi, L.; Jiang, L.; Gao, M. Numerical research on melt pool dynamics of oscillating laser-arc hybrid welding. *Int. J. Heat Mass Transf.* **2022**, *185*, 122421. [CrossRef]
165. Zhan, X.; Zhao, Y.; Liu, Z.; Gao, Q.; Bu, H. Microstructure and porosity characteristics of 5A06 aluminum alloy joints using laser-MIG hybrid welding. *J. Manuf. Process.* **2018**, *35*, 437–445. [CrossRef]
166. Wang, Z.; Gong, M.; Zhou, L.; Gao, M. A review of numerical simulation of laser–arc hybrid welding. *Materials* **2023**, *16*, 3561. [CrossRef]
167. Jiang, Y.; Meng, Y.; Chen, H.; Wu, X.; Deng, A. Effects of oscillating frequency on keyhole stability and porosity inhibition in high-power laser-arc hybrid welding of 10-mm-thick 6082 aluminum alloy. *J. Mater. Res. Technol.* **2024**, *30*, 385–396. [CrossRef]
168. Yazdian, N.; Mohammadpour, M.; Kong, F.; Kovacevic, R. Hybrid laser/arc girth welding of 304L stainless steel tubes, part 1–Pore mitigation, thermal analysis and mechanical properties. *Int. J. Press. Vess. Piping*. **2018**, *163*, 75–93. [CrossRef]
169. Cai, C.; He, S.; Chen, H.; Zhang, W. The influences of Ar-He shielding gas mixture on welding characteristics of fiber laser-MIG hybrid welding of aluminum alloy. *Opt. Laser Technol.* **2019**, *113*, 37–45. [CrossRef]
170. Panwisawas, C.; Perumal, B.; Ward, R.M.; Turner, N.; Turner, R.P.; Brooks, J.W.; Basoalto, H.C. Keyhole formation and thermal fluid flow-induced porosity during laser fusion welding in titanium alloys: Experimental and modelling. *Acta Mater.* **2017**, *126*, 251–263. [CrossRef]
171. Vorontsov, A.; Zykova, A.; Chumaevskii, K.; Osipovich, K.; Rubtsov, V.; Astafurova, E.; Kolubaev, E. Advanced high-strength AA5083 welds by high-speed hybrid laser-arc welding. *Mater. Lett.* **2021**, *291*, 129594. [CrossRef]
172. Miao, H.; Yu, G.; He, X.; Li, S.; Chen, X. Comparative study of hybrid laser-MIG leading configuration on porosity in aluminum alloy bead-on-plate welding. *Int. J. Adv. Manuf. Technol.* **2017**, *91*, 2681–2688. [CrossRef]
173. Yan, S.; Zhu, Z.; Ma, C.; Qin, Q.H.; Chen, H.; Fu, Y.N. Porosity formation and its effect on the properties of hybrid laser welded Al alloy joints. *Int. J. Adv. Manuf. Technol.* **2019**, *104*, 2645–2656. [CrossRef]
174. Leo, P.; Renna, G.; Casalino, G.; Olabi, A.G. Effect of power distribution on the weld quality during hybrid laser welding of an Al–Mg alloy. *Opt. Laser Technol.* **2015**, *73*, 118–126. [CrossRef]
175. Ola, O.T.; Doern, F.E. Keyhole-induced porosity in laser-arc hybrid welded aluminum. *Int. J. Adv. Manuf. Technol.* **2015**, *80*, 3–10. [CrossRef]
176. Hagenlocher, C.; Stritt, P.; Weber, R.; Graf, T. Strain signatures associated to the formation of hot cracks during laser beam welding of aluminum alloys. *Opt. Laser Eng.* **2018**, *100*, 131–140. [CrossRef]
177. Ivanov, M.; Cherniavsky, A.; Tingaev, A.; Bezgans, Y.; Derbenev, D.; Shaburova, N.; Suleymanova, I.; Alrukhaymi, A.; Sonar, T. Experimental and Numerical Investigation on Cold Cracking Susceptibility of Naval Grade High Strength Steel Welds for Lightweight Shipbuilding Structures. *Int. J. Lightweight Mater. Manuf.* **2024**, *7*, 597–613. [CrossRef]
178. Oana, S.-A.; Karancsi, O.; Mitelea, I.; Uţu, I.-D.; Craciunescu, C.M. The role of filler material selection in the laser welding process of deformable 6xxx series aluminum alloys. *Mater. Today Proc.* **2023**, *78 Pt 2*, 287–294. [CrossRef]
179. Wang, L.; Li, X.; Gao, M.; Zeng, X. Stabilization mechanism and weld morphological features of fiber laser-arc hybrid welding of pure copper. *J. Manuf. Process.* **2017**, *27*, 207–213. [CrossRef]
180. Tang, G.; Zhao, X.; Li, R.; Liang, Y.; Jiang, Y.; Chen, H. The effect of arc position on laser-arc hybrid welding of 12-mm-thick high strength bainitic steel. *Opt. Laser Technol.* **2020**, *121*, 105780. [CrossRef]
181. Xue, B.; Chang, B.; Wang, S.; Hou, R.; Wen, P.; Du, D. Humping formation and suppression in high-speed laser welding. *Materials* **2022**, *15*, 2420. [CrossRef]
182. Bunaziv, I.; Dørum, C.; Nielsen, S.E.; Suikkanen, P.; Ren, X.; Nyhus, B.; Eriksson, M.; Akselsen, O.M. Laser-arc hybrid welding of 12- and 15-mm thick structural steel. *Int. J. Adv. Manuf. Technol.* **2020**, *107*, 2649–2669. [CrossRef]
183. Beyer, E.; Brenner, B.; Poprawe, R. Hybrid laser welding techniques for enhanced welding efficiency. In Proceedings of the International Congress on Applications of Lasers & Electro-Optics, Detroit, MI, USA, 14–17 October 1996; AIP Publishing: Melville, NY, USA, 1996. [CrossRef]
184. Graf, T.; Staufer, H. Laser-hybrid welding drives VW improvements. *Weld J.* **2003**, *82*, 42–48.
185. Kah, P. *Usability of Laser–Arc Hybrid Welding Processes in Industrial Applications*; Lappeenranta University of Technology: Lappeenranta, Finland, 2011, ISBN 978-952-265-100-6. Available online: https://urn.fi/URN:ISBN:978-952-265-100-6 (accessed on 13 September 2024).
186. Casalino, G.; Campanelli, S.L.; Ludovico, A.D. Laser-arc hybrid welding of wrought to selective laser molten stainless steel. *Int. J. Adv. Manuf. Technol.* **2013**, *68*, 209–216. [CrossRef]
187. Lillemäe, I.; Vääräniemi, J.; Österberg, T. Fatigue strength of thin laser-hybrid welded full-scale deck structure. *Int. J. Fatigue* **2017**, *95*, 282–292. [CrossRef]
188. Petring, D.; Fuhrmann, C. Recent progress and innovative solutions for laser-arc hybrid welding. In Proceedings of the Pacific International Conference on Applications of Lasers and Optics, Laser Institute of America, Melbourne, Australia, 19–21 April 2004; Volume 2004, No. 1. [CrossRef]

189. Petring, D. Developments in hybridisation and combined laser beam welding technologies. In *Handbook of Laser Welding Technologies*; Woodhead Publishing: Cambridge, UK, 2013; pp. 478–504. [CrossRef]
190. Kah, P.; Salminen, A.; Martikainen, J. The effect of the relative location of laser beam with arc in different hybrid welding processes. In Proceedings of the International Congress on Applications of Lasers and Electro-Optics (ICALEO), Orlando, FL, USA, 2–5 November 2009. [CrossRef]
191. Welding, L.A. First application of hybrid laser-arc welding to commercial ships. *Mitsubishi Heavy Ind. Tech. Rev.* **2010**, *47*, 59.
192. Uemura, T.; Gotoh, K.; Uchino, I. Expansion of laser–arc hybrid welding to horizontal and vertical-up welding. *Weld. World* **2022**, *66*, 495–506. [CrossRef]
193. Kristensen, J.K. Trends and developments within welding and allied processes. In Proceedings of the IIW International Conference in Connection with Annual Assembly, Copenhagen, Denmark, 24–25 June 2002.
194. Ola, F.E. Fusion weldability studies in aerospace AA7075-T651 using high-power continuous wave laser beam techniques. *Mater. Des.* **2015**, *77*, 50–58. [CrossRef]
195. Vaidya, W.V.; Angamuthu, K.; Koçak, M.; Grube, R.; Hackius, J. Strength and fatigue resistance of laser-MIG hybrid butt welds of an airframe aluminium alloy AA6013. *Weld. World* **2006**, *50*, 88–97. [CrossRef]
196. Gong, M.; Meng, Y.; Zhang, S.; Zhang, Y.; Zeng, X.; Gao, M. Laser-arc hybrid additive manufacturing of stainless steel with beam oscillation. *Addit. Manuf.* **2020**, *33*, 101180. [CrossRef]
197. Gong, M.; Zhang, S.; Lu, Y.; Wang, D.; Gao, M. Effects of laser power on texture evolution and mechanical properties of laser-arc hybrid additive manufacturing. *Addit. Manuf.* **2021**, *46*, 102201. [CrossRef]
198. Liu, H.; Xu, L.; Hao, K.; Han, Y.; Zhao, L.; Ren, W. Optimizing microstructure and minimizing defects in laser-arc hybrid additive manufacturing of Al-Cu alloy: The role of laser mode. *Mater. Sci. Eng. A* **2025**, *922*, 147647. [CrossRef]
199. Liu, M.; Ma, G.; Liu, D.; Yu, J.; Niu, F.; Wu, D. Microstructure and mechanical properties of aluminum alloy prepared by laser-arc hybrid additive manufacturing. *J. Laser Appl.* **2020**, *32*, 022052. [CrossRef]
200. Li, X.; Xu, X.; Hu, X.; Shi, H.; Li, X.; Liu, W.; Gan, W.; Xu, C.; Wang, X. Microstructure and mechanical properties of Cu-Cr-Zr alloy prepared by electron beam additive manufacturing and laser-MIG hybrid welding. *J. Manuf. Process.* **2024**, *117*, 24–39. [CrossRef]
201. Ma, S.; Chen, X.; Jiang, M.; Li, B.; Wang, Z.; Lei, Z.; Chen, Y. Surface morphology, microstructure and mechanical properties of Al–Mg–Sc alloy thin wall produced by laser-arc hybrid additive manufacturing. *Thin-Walled Struct.* **2023**, *186*, 110674. [CrossRef]
202. Wang, C.; Suder, W.; Ding, J.; Williams, S. Wire based plasma arc and laser hybrid additive manufacture of Ti-6Al-4V. *J. Mater. Process. Technol.* **2021**, *293*, 117080. [CrossRef]

Disclaimer/Publisher's Note: The statements, opinions and data contained in all publications are solely those of the individual author(s) and contributor(s) and not of MDPI and/or the editor(s). MDPI and/or the editor(s) disclaim responsibility for any injury to people or property resulting from any ideas, methods, instructions or products referred to in the content.